Optimization of Design Factors for Electrospun Scaffolds

for Regenerative Medicine

by

Robert Espinoza

A Thesis Presented in Partial Fulfillment
of the Requirements for the Degree
Master of Science

Approved July 2013 by the
Graduate Supervisory Committee:

Vincent Pizziconi, Chair
Stephen Massia
Antonio Garcia

ARIZONA STATE UNIVERSITY

August 2013

ABSTRACT

The objective of this research is to investigate the relationship among key process design variables associated with the development of nanoscale electrospun polymeric scaffolds capable of tissue regeneration. To date, there has been no systematic approach toward understanding electrospinning process parameters responsible for the production of 3-D nanoscaffold architectures with desired levels quality assurance envisioned to satisfy emerging regenerative medicine market needs. , As such, this study encompassed a more systematic, rational design of experiment (DOE) approach toward the identification of electrospinning process conditions responsible for the production of dextran-polyacrylic acid (DEX-PAA) nanoscaffolds with desired architectures and tissue engineering properties. The latter includes scaffold fiber diameter, pore size, porosity, and degree of crosslinking that together can provide a range of scaffold nanomechanical properties that closely mimics the cell microenvironment. The results obtained from this preliminary DOE study indicate that there exist electrospinning operation conditions capable of producing Dex-PAA nanoarchitecture having potential utility for regenerative medicine applications.

DEDICATION

This thesis is dedicated first and above all to God Almighty for being my rock and source of refuge, and for his word in Proverbs 16:9 that kept me all through the journey of completing this work. I also dedicate this work to my grandfather Albert Espinoza, to my parents Claudia and Carlos Espinoza, my brother Felix Espinoza, and to the brothers I've made at the iron forge for being great pillars of support.

ACKNOWLEDGMENTS

I would like to express the deepest appreciation to my mentor, Professor Vincent Pizziconi, who has taught me the spirit of adventure with regard to research and scholarship. This thesis would not have been possible without his guidance and persistent help.

I would also like thank Kimia Seyedmadani, for going through this journey with me in the quest for a thesis. Dr. Stephen Massia and Dr. Christine Pauken, many thanks for your support and guidance and for all the fun times!

Finally, a special thanks to the lab team (aka the A-Team) for their assistance on the project; Joseph Heath, Jaycob Proffitt, Doug Liu, Ricardo Barrios, Luis Valenzuela, David Mazur, Colin Barry, Chongji Liu, Ouray Kinsel, Jordan Hines, Shiv Karthik, Daniel Skromme, Della Tao, Xochitl Rayas, Aleydis Estrada, Luis Laitano, Brian Trinh.

TABLE OF CONTENTS

LIST OF TABLES

LIST OF FIGURES

CHAPTER 1

INTRODUCTION

Regenerative Medicine

Since the introduction of the field of tissue engineering in the 1980s, much progress has been made toward the development of novel 3D biomaterial constructs and related biofabrication methods that are now being translated into clinically approved products to support the emerging field of regenerative medicine. One such 3D biofabrication method that has caught considerable attention in the regenerative medicine research community is electrospinning.

Electrospinning

The electrospinning process, which uses electrostatic forces to spin polymer fibers, has been around for over a hundred years. However, electrospinning has only recently gained considerable attention for being one of the preferred methods in producing tissue regenerative scaffolds due to its ability to control electrospinning fabrication process parameters with relative ease and accuracy. With electrospinning, biocompatible polymer fibers, having diameters ranging from nanometers to micrometers, can be made into porous 3D scaffolds over a wide range of pore diameters and porosity.

Considering that the extracellular matrix (ECM) in human tissue is comprised of nanoscale diameter biopolymer fibers that form complex 3D nanoarchitectures, electrospinning is an excellent fabrication process to produce multiscale, three dimensional nano- and microscale fibrous polymer architectures that can mimic the ECM's nanomechanical and biochemical transport properties. In addition, electrospun fibers can be oriented using relatively simple methods, such as, a rotating drum that provide the ability to fabricate totally random to completely oriented 3D scaffold architectures as a means to control mechanical and transport properties. For example, the more aligned the fibers are, the more the porosity decreases throughout the nanoscaffold system.

In addition, various types of polymer or composite solutions can be spun into fibers, which allow for a variation in both the physical and chemical properties of these three dimensional

structures and thus can be tailored specifically for interacting with the targeted tissue area. In turn the electrospinning process will depend upon the properties of the desired solutions.

The Extracellular Matrix

The extracellular matrix (ECM) is the physical scaffolding component for all tissues and organs in the human body. The importance of the ECM is shown through its role in how specific biochemical and biomechanical cues are initiated by the ECM that results in tissue morphogenesis, differentiation and homeostasis [12]. Even though the ECM is made up of water, proteins, and polysaccharides, each tissue type in the body has its own unique ECM with its own composition and topology that induces the specific cues needed to interact with the various cells in the system: some being; epithelial, fibroblast, adipocyte, and endothelial [12]. There are also cell to surface receptors that help adhesion, called integrins.

Cells do not just say “stick” together, but rather actually are organized into very diverse and specific patterns, depending on the type of tissue [5]. It really does depend on the type of tissue that the cell would have to integrate into, as each tissue type varies to a certain degree in physicochemical properties. This includes mechanical properties, such as, stiffness, as well as, porosity and pore size, among others.

ECM and Cell Adhesion

The underlying premise of a tissue regenerative scaffold is its ability to create a microenvironment for cellular adhesion and migration. The cellular microenvironment induces the initiation of very specific adhesion mechanisms that allow them to assemble into three dimensional connective tissues. Cell adhesion depends to a great extent on the physicochemical specifications of the microenvironment and biochemical intercellular signaling of the tissue system [18].

Optimization of Process Design Factors for PAA-Dextran Electrospun Scaffolds for Regenerative Medicine

The goal of this research project is to identify electrospinning process parameters to achieve reproducible polyacrylic acid (PAA)-dextran (Dex) electrospun scaffold structures having desired physicochemical parameters. PAA-Dex nanoscaffolds are being investigated in our bioengineering regenerative medicine research group at ASU as potential replacements for mesh support structures currently used in pelvic organ prolapse. The Design of Experiment (DOE) methodology is proposed to systematically investigate electrospun process parameters, such as, driving voltage, target distance, and polymer molecular weight and solution concentration. DOE was used to determine the effect of process parameters on desired scaffold specifications including pore size, porosity, and fiber diameter. The overall goal of this study is to identify optimal electrospun process conditions for fabricating 3-D Dextran-PAA having desired reproducible physicochemical properties.

Literature Review

A literature review was conducted to scope the current and past work on cellular proliferation in a characterized electrospun environment. The table below list the articles found on the subject were reported by researchers as to what electrospinning parameters were chosen to encourage cellular proliferation for different polymer systems tested.

Article Title	Author	Polymer(S)	Cell Type
Fabrication and Characterization of Electrospun PLGA/MWNTs/Hydroxyapatite Biocomposite Scaffolds for Bone Tissue Engineering	Hualin Zhang	PLGA, MWNTs, and HA	bone marrow-derived mesenchymal stem cells (BMSC)
Nanobioengineered Electrospun Composite Nanofibers and Osteoblasts for Bone Regeneration	Jayarama Reddy Venugopal	PCL, Gel, HA,	human fetal osteoblas (hFOB)
Nanostructured biocomposite substrates by electrospinning and electrospraying for the mineralization of osteoblasts	Deepika Gupta	PLACL, GEL, HA	human fetal osteoblas (hFOB)
Poly(lactide-co-glycolide)/hydroxyapatite nanofibrous scaffolds fabricated by electrospinning for bone tissue engineering	Lihong Lao	PLGA, HA	Osteoblasts MC3T3-E1
Preparation and Characterization of Novel Bone Scaffolds Based on Electrospun Polycaprolactone Fibers Filled with Nanoparticles	Patcharaporn Wutticharoenmongkol	PCL, CaCO3, HA	Human osteoblasts (SaOS2) and mouse fibroblasts (L929)

Table 1: Shows the literature review done on articles for cellular proliferation on electrospun scaffolds [16, 22, 25, 33, 51].

CHAPTER 2

THEORY

Thin Films and Spin Coating

Spin coating is the process of depositing a liquid solution onto a substrate and accelerating to a desired rotation per minute (RPMs) for a specified period of time. During the spin, the solution will flow radially outwards while the excess spins off of the edge of the substrate forming a thin film on the surface. The solvent in the solution evaporates leaving only a thin film of the desired polymers. The molecular weight of the solution will affect how well the solution will flow radially on the substrate, which will then be dependent on the rate of acceleration. The thinning of the film will be dependent on the spinning time, the longer the substrate spins the more the solvent evaporates and the thinner the film will become. Various models have been developed which relate spin coating thickness to spin coating process parameters. As seen in Equation 1:

$$h_f = C_0\left(\frac{e}{2(1-C_{0)}K}\right)^{\frac{1}{3}}$$

Equation 1: Shows the equation for film thickness when spinning thin films.

The film thickness is dependent on the concentration of the solution (C_0), evaporation rate of the solvent (e), and K, a system constant, that is directly proportional to the evaporation rate and the fluid density and inversely proportional to viscosity.

Film thickness can be measured by the use of an ellipsometer, by emitting a light source that becomes polarized and reflects to a detector which analyzes the light. A refractive index is then determines the thickness of the film.

Surface Tension

One of the most important factors for an implantable material is its surface energy, which is also called surface tension. Surface tension is the measure of free energy over a unit area of a surface [35].

The Young-Dupre equation (as shown in Equation 2) is used to calculate the surface tension of the liquid to solid interface by taking into account the contact angle of the liquid on the solid surface.

$$\Upsilon_{SG} = \Upsilon_{SL} + \Upsilon_{LG}*\cos\theta$$

Equation 2: Young Dupre Equation, used to calculate surface tension.

The symbol Υ_{SG} represents the surface tension between the solid and gas interface. Υ_{SL} would then represent the surface tension between the solid and liquid interface, while Υ_{LG} surface tension between the liquid and gas interface of the droplet dropped onto the surface material. The θ is found by measuring the angle on the droplet as shown in figure 4, which was found using a goniometer.

The tension of a surface can be used to determine how well a droplet wets the surface. It has also been shown that there is a specific range of surface tension that promotes cellular adhesion which leads to a desired rate of cellular proliferation and differentiation [21]. How cells or liquids react to the surface tensions can be seen visually by how well it spreads out on the surface. The more wetting occurs over a larger spread area, the greater the adhesion forces are to the cohesive forces on the surface, and the opposite occurs for when non-wetting where the adhesion forces are less than the cohesive forces. Wetting can also be shown by measuring the contact angles brought about by wetting or non-wetting, where a droplet of a liquid is placed on a solid surface. The droplet would either spread out or re-track on the surface area. At 0 degrees the wetting is considered completely spread on the surface, any other angles less than 90 degrees would be considered as wetting, but any degrees greater than 90 degrees would prove to be non-wetting. Wetting would occur on when the surface tension of the liquid is lower than the surface tension of the surface material, and the larger the difference in surface tension between the liquid and solid, the easier it would be for the liquid to spread about the surface.

Electrospinning Theory

The electrospinning system consists of a syringe pump that is filled with a polymer solution. A high voltage source is utilized to induce a certain polarity into the polymer that allows

the polymer droplet to exceed adhesion forces and be propelled through the air onto a collection plate that has been induced with an opposite polarity [37]. While the polymer is airborne, the solvent in the solution evaporates leaving the polymer that solidifies almost instantly. The electric field that is produced by the high voltage supply has to become greater than that of the surface tension of the solution in order to allow the fiber jet to pass through an effect called the Taylor cone [37].

Equation 3 is used to describe the process of electrospinning scaffolds under a set of specific variables. By understanding how each variable can affect the scaffold properties, the user is able to produce the desired scaffold properties on demand. In this equation the variables are as follows:

$$V_C^2 = \frac{4 * H^2 * [Ln\left(\frac{2L}{R}\right) - 1.5] * (0.117 * \pi * R * \Upsilon)}{L^2}$$

Equation 3: Shows the equation used for electrospinning [14].

- V_C = The voltage applied to the system
- H = Air gap distance between the syringe needle tip and the collection plate
- R = The inner radius of the syringe needle
- L = The length of the needle barrel
- Υ = The surface tension of the solution

Figure 1 (below), shows a visual representation to how the variables from equation 3 relate to the electrospinning process.

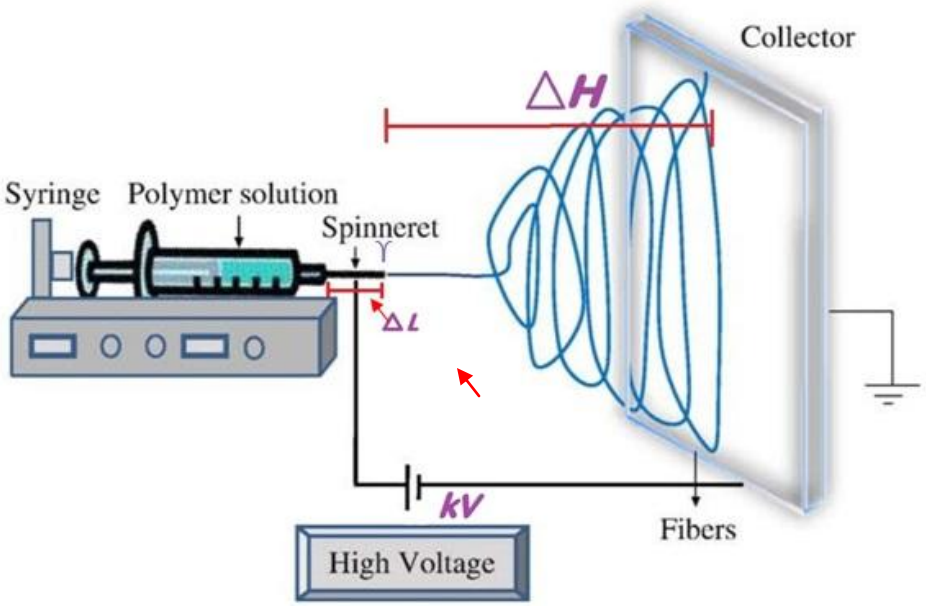

Figure 1: Shows the relationship between the electrosinning setup and the variables from equation 2 [Adapted from [4]].

The Taylor cone occurs with a droplet at the tip of the needle of the syringe, where its stability depends on the relationship between the charge on the solution and the surface tension. When the droplet can be raised to a specific potential the droplet is able to elongate until it takes the shape of a cone [48]. The droplet also has to reach a certain half angle that will allow the Taylor cone to form, allowing for the fiber jet to shoot a stream across a distance onto a collection plate. The viscosity of the solution also plays an important role, since the lower the viscosity the easier it is for the droplet to be emitted from the tip of the cone [48]. It was also shown by Doshi and Reneker that with a specific conductivity of 400 µS, the jet would break below a viscosity of 800 centipoise and anything above 4,000 centipoise the fibers would have a difficult time forming due to the solvent in the solution drying up quicker before it has a chance to come off the tip of the syringe and take flight [16]. The increase of the electric field to compensate for the higher viscosity would also cause a destabilization in the jet stream. The tip of the needle is not the only important part of the system. Other factors that affect the jet stream are its; path length, area along in the path length, the rate at which the syringe pump pumps the solution, and the relationship of the voltage level that allows the solution to be jetted through the air.

By understanding the relationship between the electric field and the electrospinning jet, new ways have been found to orient the fibers to desired specifications [41]. The collection plate is another important feature of the electrospinning process which allows the precision and control needed to orient the fibers. Currently there are several models of these plates that allow the desired fiber orientation. By using rotating drums the fibers can be highly aligned and a large area can also be produced. Wires can also be applied to the drum collectors to set the desired geometrical scaffold area. The rotation speeds of these drums have a direct impact on the fiber alignment. At lower speeds the fiber alignment tends to be random, but as the speed increases the fibers become more significantly aligned with each other. Something to note, however, is that at high enough rotation speeds, the fibers start to take on damage and even break. What leads to this outcome is that as the rotation speed increases, the fibers solidify at a faster rate becoming more amorphous.

Another type of set up involves the use of electrodes, which by placing them in a certain configuration allows fibers to be directed onto the collection plate, thus resulting in improved fiber alignment. There is more than one way to set up electrodes, and each method has their own pros and cons. By winding a wire onto a drum, the fibers can be aligned during the rotation of the drum. The set up is relatively simple and produces highly aligned fibers. A limitation of this set up only produces the fibers on the wire instead of on the whole range of the drum. Electrodes can be placed in parallel, which is simple to set up and can produce highly aligned fibers that can be easily transferable to another substrate [42]. The limitation for this set up would be that thicker layer scaffolds will not be possible and the length of the aligned fibers would also be limited as well. An array of counter-electrodes in parallel can also be simple to set up, but the pattern throughout the fiber mesh will not all be the same, making this method inconsistent and unreliable. Another limitation to this set up is seen over time when the fibers set in a random alignment, which could be due to residual charges on the deposited fibers that distort the electric field profile [42]. Static electrodes, that are stationary and do not rotate, can also be used to collect the electrospun fibers through the air.

Solutions have specific conductivities that can influence the diameter of the fibers within 1-2 orders of magnitude [37]. There is a direct relationship between the conductivity and the charge that is allowed to be applied to the solution. As the conductivity increases so will the charge carrying capacity also increases. Solutions with high conductivity have been shown to have problems in strong electric fields that result in inconsistent fiber diameters. There is also a relationship between the conductivity and the radius of the fiber jet, where the fiber jet is found to be related to the cube root of the solution conductivity [37]. The conductivity can also be altered by the addition of NaCl, which is a simple way to introduce ions into the solution that will increase the net charge density that in turn will increase the electric force on the jet and decrease the fiber diameters.

Electrospinning Parameters

Understanding the interactions between the variables in equation 3 allows the user to be able to control their system to a high degree. The overall goal is to determine how the independent variables in equation 3 would affect the dependant variables of fiber diameter, pore sizes, fiber orientation, and mechanical properties.

Pore sizes remain as one of the most important factors determining the functionality of the scaffold. The pore sizes will ultimately set the ranges of porosity throughout the system creating the surface area-to-volume ratios that would directly affect the way the cells would interact with their environments and produce the needed amount of connective tissue at a timely rate. Pore symmetry, or the path of the pores through the structure, also influences cellular migration throughout the system.

Literature Review of Design of Experiments (DOE)

A literature review was conducted specifically on the design of experiments (DOE) for the process parameters of electrospinning. Even though the polymer types varied in these studies, there existed universal processing parameters that directly affect fiber diameter and pore diameters. By determining the relationship of these process parameters to fiber specifications, it may then be possible to optimize the design factors to obtain electrospun scaffolds suitable for regenerative medicine.

#	Title	Authors	Independent Variables Tested	Notes
1	A new approach for optimization of electrospun nanofiber formation process	Mohammad Ziabari, Vahid Mottaghitalab, and Akbar Khodaparast Haghi†	kV, Distance, Flow Rate, Concentration	shows multilpe interactions between variables
2	Effects of electrospinning parameters on polyacrylonitrile nanofiber diameter: An investigation by response surface methodology	O.S. Yo¨rdem 1, M. Papila *, Y.Z. Mencelog˘lu 2	Concentration, kV, Distance	Concentration, kV, and Distance were found to be significant variables
3	Investigation on Process Parameters of Electrospinning System through Orthogonal Experimental Design	Wenguo Cui, Xiaohong Li, Shaobing Zhou, Jie Weng	kV, Concentration, Molecular Weight, Solvent, Flow Velocity, Nozzle Size	Shows the significant variables being molecular weight andconcentration
4	Regeneration of Bombyx mori silk by electrospinning—part 1: processing parameters and geometric properties	Sachiko Sukigaraa, Milind Gandhib, Jonathan Ayutsedec, Michael Micklusd, Frank Ko	Concentration, kV, Distance	States that the Concentration is the dominant parameter
5	Regeneration of Bombyx mori silk by electrospinning. Part 2. Process optimization and empirical modeling using response surface methodology	Sachiko Sukigaraa, Milind Gandhib, Jonathan Ayutsedec, Michael Micklusc, Frank Ko	Concentration, kV, Distance	Contour plots relating fiber diameter to electric field and solution concentration were generated
6	A Design of Experiments (DoE) Approach to Material Properties Optimization of Electrospun Nanofibers	Stuart R. Coles,1 Daniel K. Jacobs,2 James O. Meredith,2 Guy Barker,3 Andrew J. Clark,1 Kerry Kirwan,2 Jon Stanger,4 Nick Tucker	Concentration, kV, Distance, Salt (Conductivity)	there is no interaction between electrostatic potential and distance. In general, there are limited interactions of no statistical significance between concentration and collection distance
7	An Investigation of Process Parameters to Optimize the Fiber Diameter of Electrospun Vascular Scaffolds through Experimental Design	Faculty Advisor: Kristen O'Halloran Cardinal, PhD Senior Project Steffi Wong ENGR 462 Fall 2010	Concentration, Voltage, Gap Distance, Flow Rate	Full Factorial Design
8	Process Optimization and Empirical Modeling for Electrospun Poly(D,L-lactide) Fibers using Response Surface Methodology	Shu-Ying Gu†,*, Jie Ren	Concentration, kV	Fibers with diameter ranging from 350 to 1900 nm
9	Fabrication of electrospun poly(methyl methacrylate) nanofibrous membranesby statistical approach for application in enzyme immobilization	* Jyh-Ping Chen , Kuo-Hsu Ho, Yi-Ping Chiang, Kuo-Wei Wu	Concentration, Distance, Temperature, Flow Rate, and Voltage	Predicted fiber diameters were in agreement with the experimental results
10	Prediction of Electrospinning Parameters for Targeted Nanofiber Diameter	Onur Sinan Yördem (sinanyordem@su.sabanciuniv.edu) Melih Papila (mpapila@sabanciuniv.edu) Yusuf Mencelolu (yusufm@sabanciuniv.edu)	Molecular Weight, Concentration, Voltage, and Distance	The response surfaces showed that there is a negative correlation between scatter defined by the coefficient of variation and the fiber diameter.

Table2: Shows the articles found for the literature review for electrospinning DOE. Several process parameters were tested showing their interactions and their relationships to fiber diameter [7, 8 ,17, 39, 46, 50, 52].

CHAPTER 3

EXPERIMENTAL METHODS

Overview

The overall goal of the experimental design and associated test systems described herein was to test specific variables that would allow electrospinning a range of desired scaffold properties. This required the design of a series of experiments that, together, sought to identify the electrospinning process conditions that, when employed, would allow the fabrication of PAA-Dextran nanoscaffolds having reproducible properties and structures within an acceptable level of quality assurance. If successful, then it will be possible to employ a more rational design of electrospun PAA-Dextran scaffolds having ranges of desired reproducible and testable properties to investigate the complex cell-biomaterial-3D micro-environment interactions that may be exploitable for tissue engineered, regenerative medicine applications.

Materials*:*

The focus of this study was to optimize the electrospinning process operational conditions for the reliable development of a degradable PAA-Dextran polymer scaffold system developed previously at Arizona State University. As such, the experimental study began with PAA and Dextran base polymers of various molecular weights.

Dextran (70 kD Mw) was purchased from Sigma-Albrich (St. Louis, MO). Dextran (500 kD Mw) was purchased from Alfa Aesar (Ward Hill, MA). Poly(acrylic acid) (60 kD Mw, purity < 35 wt%) was purchased from Polysciences Inc. (Warrington, PA). Five samples of Stainless Steel 2B 316L, supplied as 3x2 inch flat sheets, were also purchased from OnlineMetals.

Preparation of PAA and Dextran Solutions for Thin Film Fabrications

Polymer solutions comprised of PAA (8.4v/v%) and Dextran (40wt%) were prepared for thin film fabrication for later use in contact angle measurements described in more detail below. Designated masses of dextran and poly(acrylic acid) in DI water and dissolved over night using a table top shaker at room temperature. The dextran solution concentration used to make thin films was set at 40 wt% for both dextran molecular weights of 70kD and 500kD. The PAA (MW~60kD) solution concentrations used to make thin films was 8.4v/v%.

Dextran and PAA Thin Film Fabrication:

Solid thin films of Dextran and PAA were fabricated using thin film spinning techniques and then stored in a controlled environment for use in contact angle measurements. Thin films of Dextran and PAA were prepared using a spin coater (Specialty Coating Systems Inc., model P-620-4-A) that was operated in a chemical hood. This spin coater has 2 spinning disks upon which to place the substrates; the smaller spin coater disk had a diameter of 1.75 inches while the larger disk having a diameter of 3.25 inches. The smaller disk would be used for solution having lower viscosity ranges, and the larger disk utilized for the higher viscosity ranges.

Clean 316L stainless steel flat substrates or glass cover slips were placed dead center on a spin coater disk set initially at rest and placed under vacuum to prevent substrate movement. Vacuum was provided to the spin coater from a vacuum source located in the hood (yellow spout).

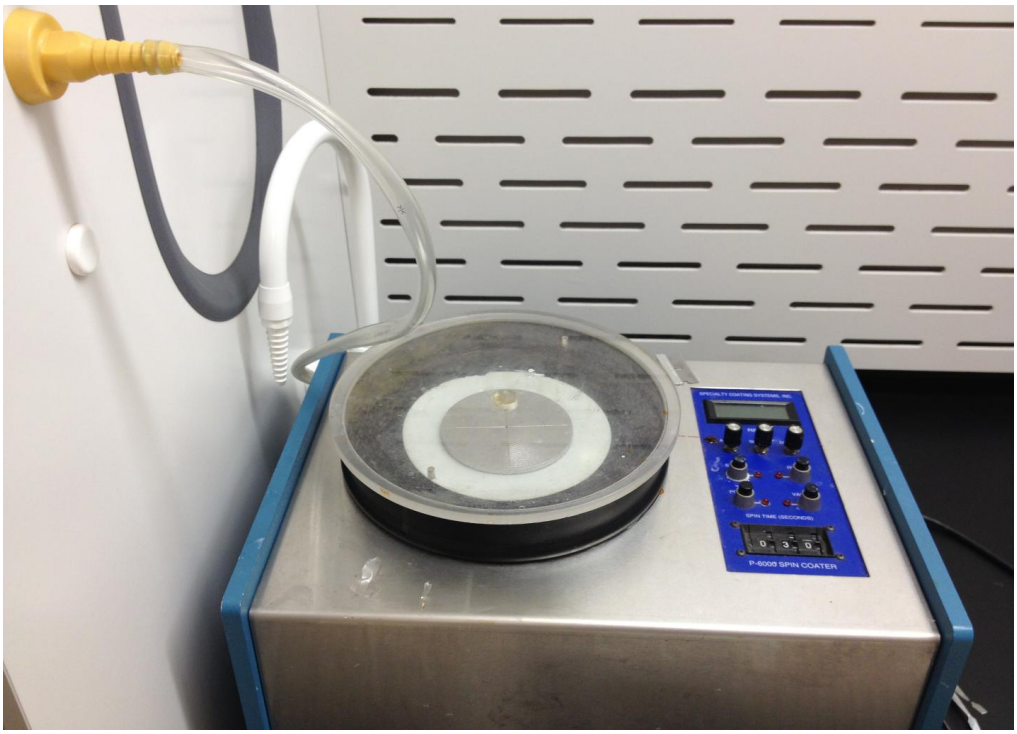

Figure 2: Spin Coater used to produce thin dextran and PPA films. Vacuum source used to hold down substrates shown as yellow valve connected to a flexible Tygon tube from the back of the spinner.

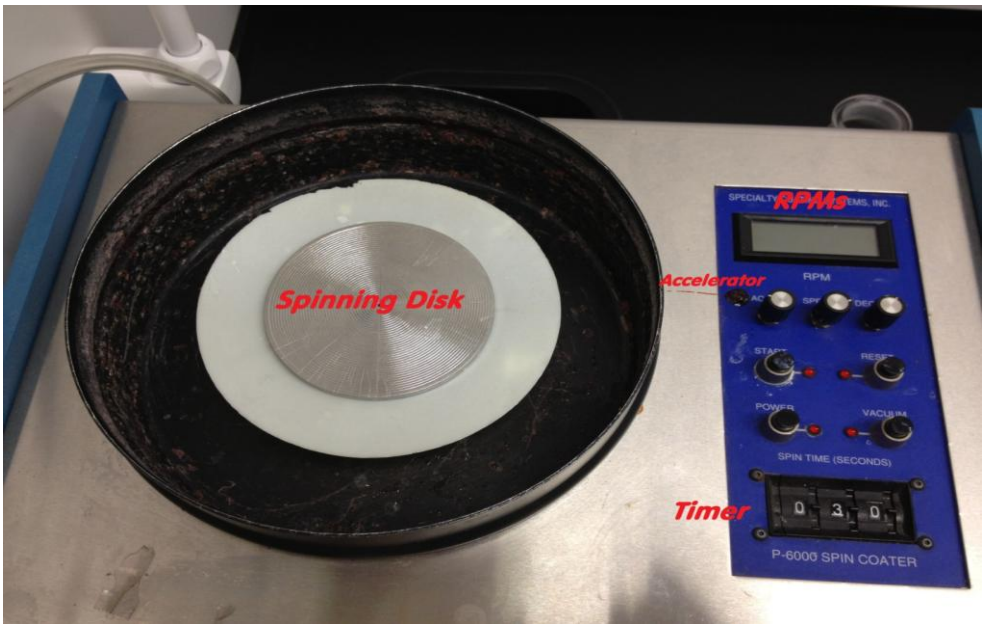

Figure 3: Thin film process parameters used in spin coating. The process variables employed for thin film spinning were time and acceleration. RPM kept constant at 6,000. A spin coater lid (not shown) was used to cover the area where the spinning disk occurred for safety measure.

PAA and Dextran Thin Film Fabrication

Thin solid polymer Dex and PAA films were fabricated for contact angle determination studies. Five polymer solutions, comprised of PAA or dextran alone or in combination, were used to produce solid thin films using a spin coater with preselected spin conditions. Polymer solutions were drawn in a 10mL disposable plastic syringe (BD, Beckton Dickinson, NJ) equipped with a 20 gage hypodermic needle. Pre-selected volumes, comprised from 8, 12 or 16 drops of polymer solution, were then transferred onto a clean glass cover slip that was previously placed onto the spin coater and held in placed by vacuum. The micro slides were cleaned by immersing them acetone for 30 minutes, while being sonicated at the same time using an Ultrasonic Homogenizer.

Figure 4: Ultrasound Sonicator and settings used to clean the surfaces of glass microslides.

For the PAA or Dex 70kD solutions, the glass cover slips were 18mm^2, but for the higher viscosity and higher molecular weights using Dex 500kD, the microslides used were 24x40mm. Table 1 indicates the number of drops that were placed on the glass cover slip for a given polymer solution.

Solution	Drops		
Dex 70 KD	8 Drops	12 Drops	16 Drops
Dex 500kD	8 Drops	12 Drops	16 Drops
PAA	8 Drops	12 Drops	16 Drops
Dex 70kD-PAA	8 Drops	12 Drops	16 Drops
Dex 500kD-PAA	8 Drops	12 Drops	16 Drops

Table 3: Indicates the amount of drops placed on glass micro slides for thin film fabrication.

Spin coater speed (RPM) was kept at 6,000 RPM fall the thin film studies. Note that the spin time and initial spin coater acceleration rate varied depending on solution viscosity (qualitatively estimated).

Goniometry Analysis and Contact Angle Determination

A Rame-Hart contact angle goniometer test system (model 100, Rame-Hart Instrument Co, NJ) shown in Figure 4a was used to measure the contact angle of designated polymer and stainless steel substrates. Procedurally, the contact angle, formed by the deposition of an aqueous sessile drop of test fluid (e.g., distilled water, polymer solutions, etc.), using BD plastic disposable syringe capped with a 20 gage hypodermic needle, was determined. The angle that forms between the sessile drop that was in 'contact' with the surface of a designated solid substrate and the horizontal plane of a substrate pertinent to this study, was measured with the Rame-Hart goniometer system as shown in Figure 5 using well known techniques reported elsewhere.

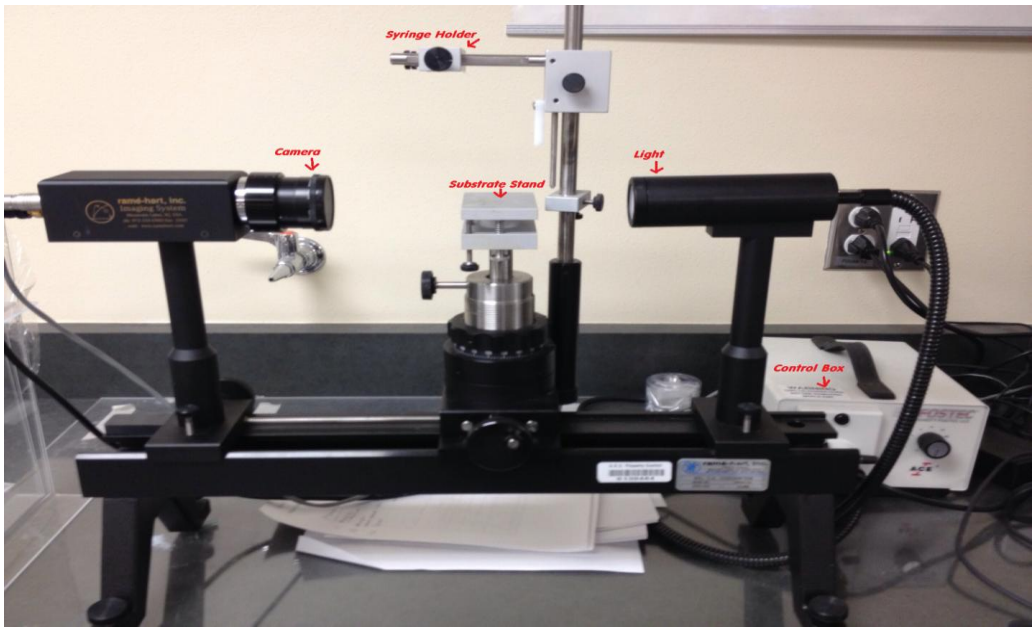

Figure 5: Goniometer used for measuring contact angles.

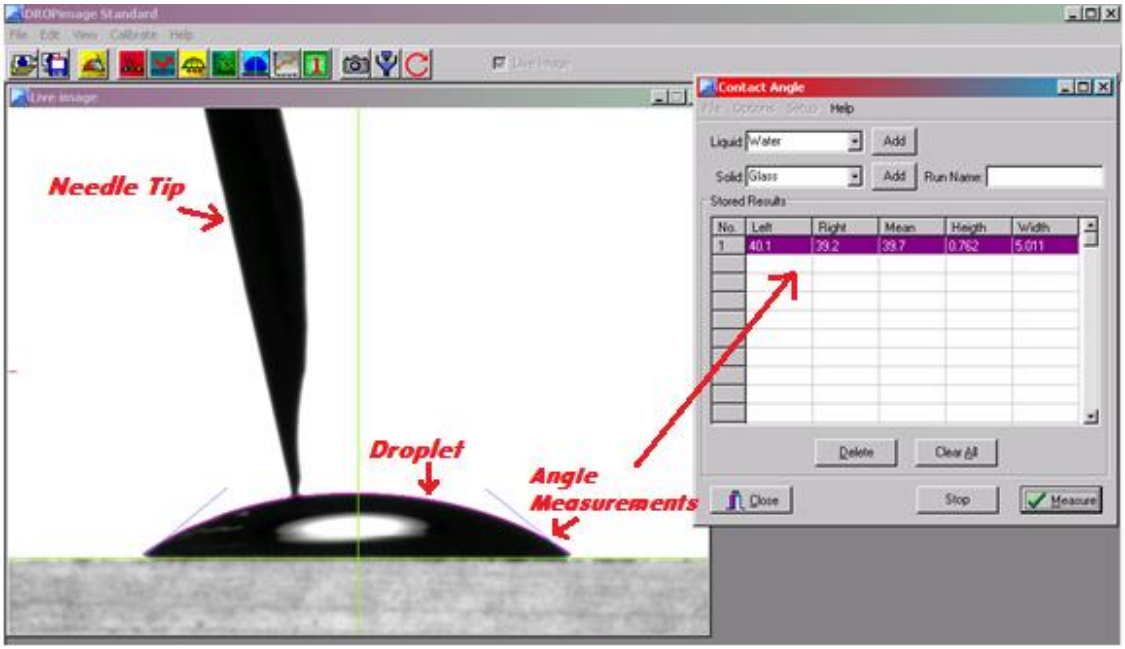

Figure 6: Depiction of contact angle measurement of droplet; input to software algorithm. Contact Angle Determination-Polymer Solution on Stainless Steel Substrates

Prior to contact angle determination, the surfaces of the stainless steel substrates were cleaned while being immersed in acetone and sonicated at the same time for 30 minutes. Once cleaned, the steel samples were analyzed using a goniometer. The solutions chosen for contact angles are shown below in table 2.

Solution	PAA% Concentration	Dextran Concetration
500kD/PAA	1	40wt%
500kD/PAA	2	40wt%
500kD/PAA	3	40wt%
500kD/PAA	4	40wt%
500kD/PAA	5	40wt%
500kD/PAA	6	40wt%
500kD/PAA	7	40wt%
500kD/PAA	8.5	40wt%

Table 4: Shows the Dex-PAA Solutions made to measure the contact angles on the stainless steel 316B L flat samples

Fabrication of PAA–Dextran 3-D Scaffolds Using Electrospinning

Electrospinning was performed with the same system and scaffolds developed used the same general procedure developed by Massia et al reported elsewhere [Mas]. The electrospinning system depicted in Figures 5a and Figure 5b , comprised of a programmable infusion pump equipped with syringe and needle accessory of pre-selected capacity/size, a conductive target, and a high voltage supply (Glassman High Voltage, Series EH), was placed in a laminar flow hood to minimize particle contamination.

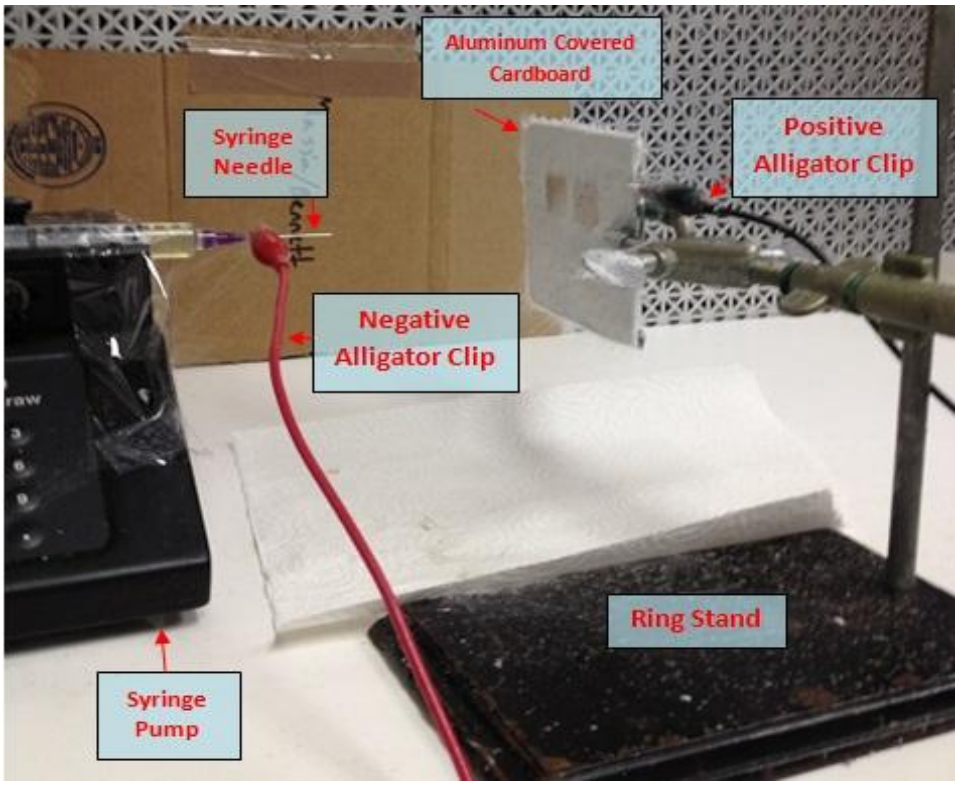

Figure 7: Shows the Electrospinning Set up.

In operation, a pre-determined voltage, set for a specific air-gap distance and polymer solution, was applied to the conductive capillary syringe tip with an alligator clip (negative) and another alligator clip (positive) was connected to the target plate that was made conductive by placing aluminum foil over the target support. The electrospun test system allows the target to be placed at pre-selected ‘air-gap’ distances (9cm, 12cm, 15cm) away from the syringe tip as depicted in Figure 6a. A designated polymer solution, e.g., dextran in PAA and DI water, typically

prepared overnight to allow for complete dissolution of the polymer in the aqueous medium was loaded into a 10 ml BD syringe capped with a 21 gauge stainless steel flat tip capillary to stabilize the so-called 'Taylor cone' as described in the Theory section. Using the programmable syringe pump (Harvard Apparatus, Model: PHD 200), the polymer solution was pumped out though the syringe at a constant volumetric rate of 10 µL/min.

Figure 8: Shows the power supply used to supply the voltage for the electric field to spin the fibers across the air gap. The current dial was set at 1 at all times during spinning, while the voltage dial was used to control the voltage output.

Prior to fabricating Dex-PAA nanoscaffolds, a series of necessary scoping experiments were implemented to determine operative electrospinning conditions that would consistently result in desired 3-D nanoscaffold architectures, i.e., crosslinkable nanofilaments absent so-called 'beading'.

Electrospinning - Scoping Experiments

An initial series of electrospinning scoping experiments were performed to empirically determine operational conditions form the otherwise complex relationship between the applied voltage, air-gap distance and polymer rheological behavior in an uncontrolled humidified environment. Figure 6 below visually depicts the electrospinning scoping strategy utilized to empirically determine operating conditions to minimize scaffold 'beading'.

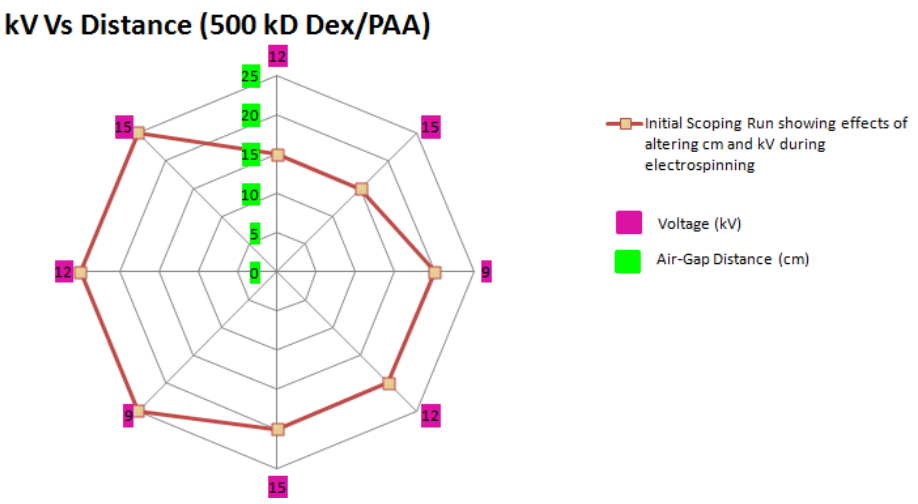

Figure 9: (Red) Shows initial electrospinning map to achieve scaffolds with minimal beading.

Preparation of Electrospinning Dex-PAA Polymer Test Solutions

Dex-PAA polymer solutions were made of various designated PAA concentrations (7%, 8.5% and 10%) with a fixed Dex concentration of 40 wt% (relative to the PAA-water mixture) that were dissolved in DI water. The DI water was available to the BioInspired Research Laboratory via a dedicated feed line from a centralized DI water source on the main ASU Tempe campus. The molecular weights used to make the Dex-PAA polymer solutions were 500kD for dextran and 60kD for PAA. The solutions were placed on a shaker for 2 days at room temperature. Once mixed, the solutions were then placed in a refrigerator to reduce bubble formation prior to electrospinning.

Electrospinning Target Collector Plate Preparation

The collector plate, designed using a 4x4 inch cardboard backing, was carefully wrapped in aluminum foil in order to minimize wrinkles that may interfere with desired scaffold deposition and integrity. In addition to the scaffold deposited directly onto the aluminum target, gold-coated conductive glass slides, were placed into slits made into the aluminum target with an x-acto razor blade. Two glass slides previously coated with gold with a thin film sputter deposition system located in the Goldwater Materials Facility of the Center for Solid State Sciences (CSSS) and

were placed on the aluminum foil and inserted into the slits that were made with a razor blade. The gold coated glass slides were placed at approximately the middle section on the top side of the collector plate. The collector plate, comprised of aluminum and gold coated sub-target areas, was then ready for electrospinning.

The target plate, clamped at its left upper corner by a gripper that was fastened to a ring stand, was held in a vertical position and aligned directly in front of the 'flight path' of the stream of polymer droplets that were propelled from the syringe via forces induced by the electric field that exceeded the interfacial surface tension forces between the polymer droplet and the stainless steel syringe. The 'positive' alligator clip connected the power supply to the upper right hand corner of the target collector plate.

Electrospinning of Dex-PAA Nanoscaffolds

The results of the early electrospinning scoping experiments suggested that the preliminary electrospinning map shown in Figure 6 needed to be further refined to achieve scaffolds with minimal beading. In particular, the determination of the interfacial surface tension between the electrospun Dex-PAA droplets of each designated concentration depicted in Table 2 in contact with the solid stainless steel substrate syringe needle was used to further refine the electrospinning process conditions determined from Equation 2 discussed in the Theory section to achieve desired nanoscaffold architectures. This resulted in a refined electrospinning process map for each Dex–PAA polymer solution utilized in making nanoscaffolds and reported in the Results section

Design of Experiment (DOE) Research Plan

It is well known in the literature that the overall morphology of electrospun scaffolds are affected by the following process parameters: viscosity, conductivity, solution concentration, polymer molecular weight, surface tension, humidity, temperature, among others.

After conducting an extensive literature review on the design of experiments DOE) for electrospinning, the minimum and maximum limits for each of the chosen process variables used to make scaffolds in this study were selected that would have the greatest effect on scaffold

architecture parameters, such as, fiber diameter, porosity, pore size among others. This included PAA concentrations kept in the range of 7-10%, while the air-gap min and max distances set between 9-15cm as shown in Table 3.

Run #	PAA% Concentration	Distance (cm)	kV
1	7	9	
2	7	12	
3	7	15	
4	8.5	9	
5	8.5	12	
6	8.5	15	
7	10	9	
8	10	12	
9	10	15	

Table 5:DOE Factors and Levels Air-Gap Distance and Applied Voltage and PAA concentration.

From Equation 2, the constitutive electrospinning relation to produce viable Dex-PAA scaffolds, was then used to determine the appropriate voltage (kV) for each DEX-PAA system utilized. As seen in Table 5, each electrospinning test system required a specific voltage gradient for a given air-gap distance and interfacial surface tension for a given flow rate provided by the test system accessories, i.e., syringe needle type, diameter and length characteristics utilized.

Run #	PAA% Concentration	Distance (cm)	kV
1	7	9	9.4
2	7	12	12.5
3	7	15	15.6
4	8.5	9	10.1
5	8.5	12	13.4
6	8.5	15	16.8
7	10	9	11.5
8	10	12	15.4
9	10	15	19.6

Table 6: Shows the DOE for electrospinning with variables PAA% Concentration, Air-Gap Distance (cm), and Voltage (kV).

Dex-PAA Nanoscaffold Post-Electrospinning Cross-Linking

Dex-PAA electrospun scaffolds were subsequently cross linked post –electrospinning using thermal dehydration techniques. Two small square samples were cut out from the bottom middle of the electrospun scaffold. The fibers were dried in a vacuumed desiccator for a minimum of 24 hours. Once dried the fibers were immediately taken from the desiccator to an oven. This was done quickly to minimize exposure to the air and keeping the fibers dry. The vacuum oven was pre-heated to 180 degrees Celsius, where the fibers would then be placed in the oven for 1 hour. After cross linking, the 1st cross linked sample was used for SEM imaging, while the 2nd sample from the same scaffold was used for FTIR analysis.

Fast Fourier Transform Infrared Spectroscopy (FT-IR)

The determination of crosslinking of the Dex-PAA fibers was determined by FT-IR spectroscopy. A Thermo Nicolet Nexus 470 FT-IR spectrometer system, available in the Goldwater Materials Facility in the CSSS at ASU, was used for this analysis FT-IR was performed on the nine scaffold runs summarized in Table 1. The sample thickness was chosen with a deposition of 1.5mL of solution spun during electrospinning to ensure optimal measurement readings.

Scanning Electron Microscopy (SEM) of Dex-PAA Nanoscaffolds

SEM images of Dex-PAA nanoscaffolds were obtained using an FEI XL-30 EFSEM. This imaging process was used for both the pre-crossed linked and crossed linked scaffold samples. From each scaffold run, 3 samples with an average area around 10x10 mm were cut from the top right area of the scaffold. From there the samples were taped unto a stub that would later be inserted into the FEI XL-30 for imaging, but before imaging, the scaffold sample on the stub were coated with gold particles to enhance the brightness of the images and ensure peak visualization of the spun fibers. The samples were coated in a Denton Vacuum (Gold Sputter) for 120 seconds.

The settings on the FEI XL-30 used to capture the images were set with; Voltage ranging from 10-15kV, a spot size of 3, and a magnification ranging from 2,000-2,500x. The scale range was set to 10 um, allowing for an average of 2,900 um^2 area to be analyzed.

ImageJ Analysis of Dex-PAA Nanoscaffolds

The analysis of fiber diameter, porosity, and morphology were measured from the SEM images using image processing software (ImageJ). Fiber diameters and pore areas were measured using ImageJ. The SEM images were set from the pixel scale to um, which was done by drawing a line over the length of the scale bar then by going to “Set Scale” under the “Analyze” tab. From there you can set the relationship between the um scale bar and the pixel lengths running across the images. Once the scale has been changed, then the measurements can begin, beginning with the fiber diameter where a line is drawn across the diameter of the fiber and “Ctrl M” is clicked to measure the length. For the pore area, the “Polygon Selections” on the tool bar was used to draw a line in between the selected surface fibers, and again by clicking “Ctrl M” the area in the pore can be measured. The fibers that were selected for analyzing were those visually seen to be closest to the surface. Any fibers seen to be underneath the top surface layer were ignored.

CHAPTER 4

RESULTS

Measuring Contact Angles

Three thin films were analyzed at a time for their contact angles and averaged to determine the average contact angle.

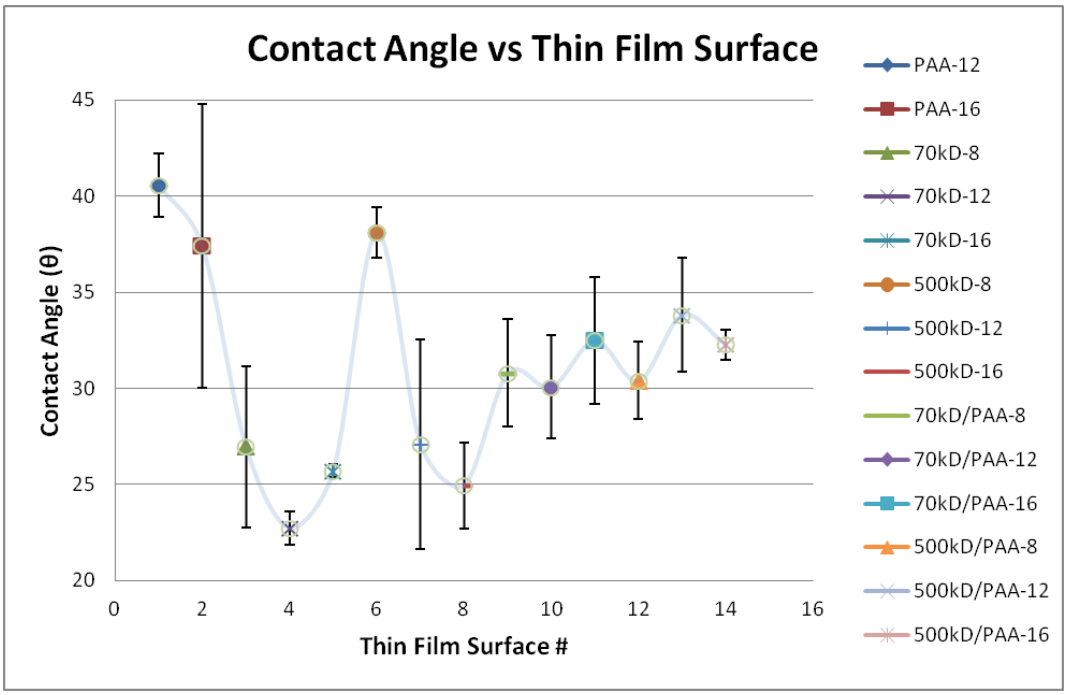

Figure 10: Shows the contact angles measured on polymer thin films. The legend details the thin film polymer spun, and how many drops of the solutions was dropped unto a glass micro-slide surface using a 21 gauge syringe needle.

Calculating Surface Tension

Table 7, below, shows the surface to gas (Y_{SG}) surface tensions for the Dextran and PAA polymers. The water surface tension was that of the Liquid-Gas (Y_{LG}) Interface. What was then calculated was the Solid-Liquid (Y_{SL}) interface of the water droplet and the surface of the polymers.

Liquid	Surface Tension (mN/m^2)
Water	72.8
Dextran 70 KD	72.16
Dextran 500 KD	72.3
PAA	65

Table 7: Shows the surface tensions for Dextran & PAA at the Surface-Gas interface, while the surface tension of water is given at the Liquid-Gas interface [6,20,35,43].

Once the surface tension was calculated, the findings were then plotted versus the polymer type and how many drops of each polymer was placed unto a micro slide when using the spin coater to spin the thin films.

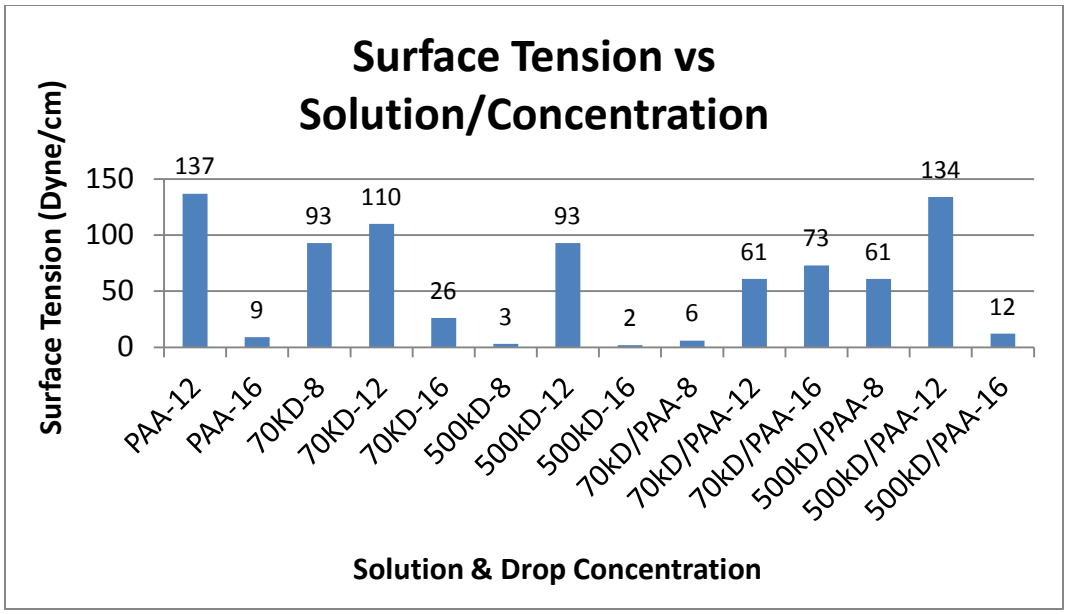

Figure 11: Shows the surface tension calculated from distilled water contact angles on the polymer surfaces of PAA, Dextran 70kD & 500kD, and mixtures of PAA and DEX 70kD & 500kD.

Contact Angle Measurements on Stainless Steel 316B L Samples:

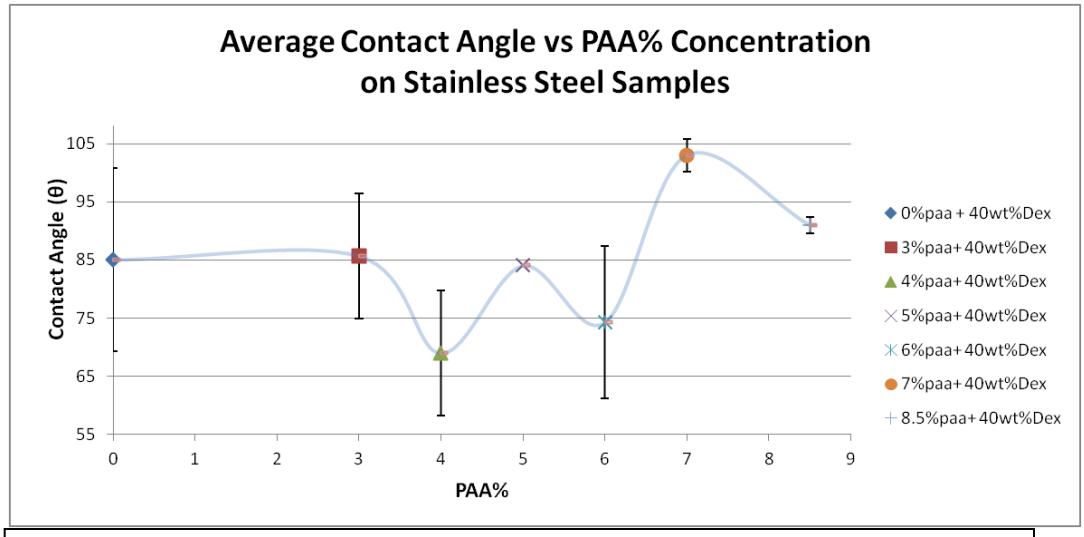

Figure 12: Shows the contact angle measured on stainless steel for solutions of Dex 40wt% with varying PAA concentrations from 0-8.5%. One drop per solution was placed unto the stainless steel surfaced, then was measured using a goniometer.

Surface Tension calculations of solutions on Stainless Steel 316B L Samples:

PAA%	Solution	surface tension of Stainless Steel	Surface Tension of Dextran 500kD	Ave Contact Angle	Surface Tension Calculation
7	500kD/PAA	43	72.3	103	99.55529334
8.5	500kD/PAA	43	72.3	91	114.8927674

Table 8: Shows the Surface Tension calculations on stainless steel for solution of Dex 40wt% and 7-8.5% PAA concentrations.

Voltage (kV) calculation for 10% PAA concentrated solutions were done by first measuring the contact angles of the PAA% concentrations of 0, 3, 4, 5, and 6% on the steel samples. The surface tension of the solutions between the surface-liquid interfaces was then calculated using the young Dupree equation. Lastly the Voltage (kV) was calculated by taking the surface tension and using it in the electrospinning equation. Once the data was found, the calculated kV was graphed vs the PAA% concentration, which produced a threadline that was used to assume what the kV would be for a 10% PAA concentration for each specific air-gap distances of 9, 12, and 15cm.

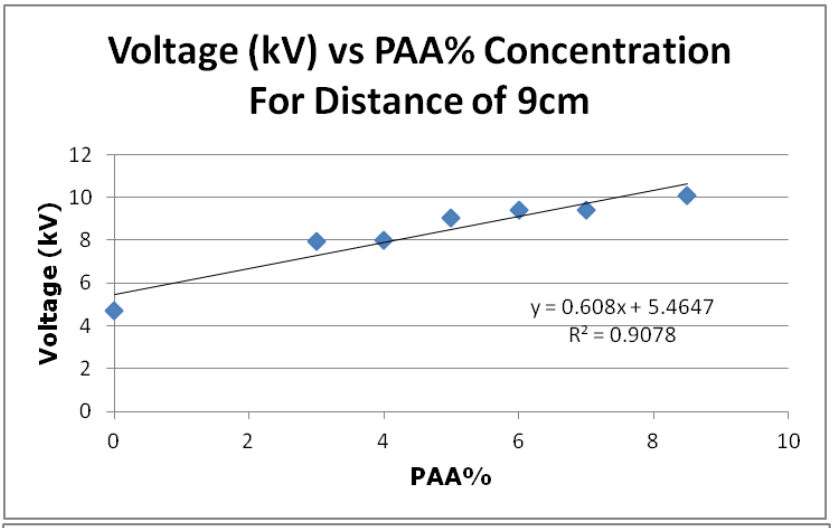

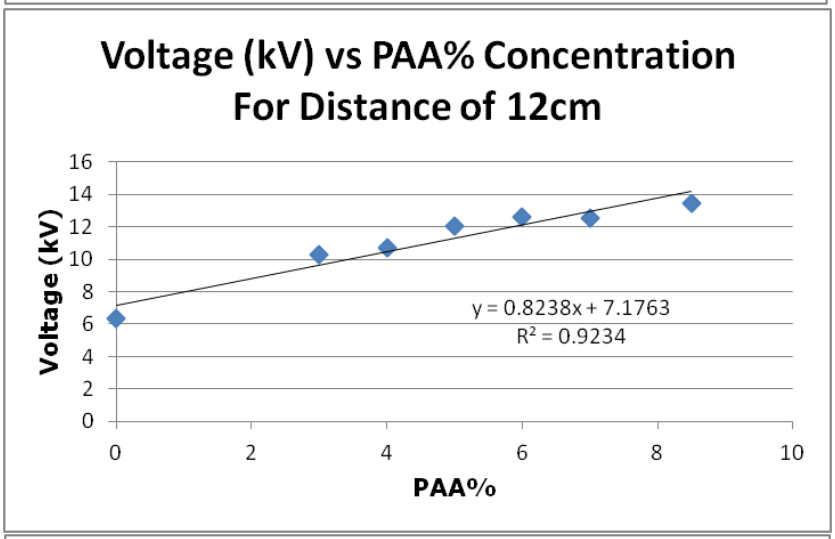

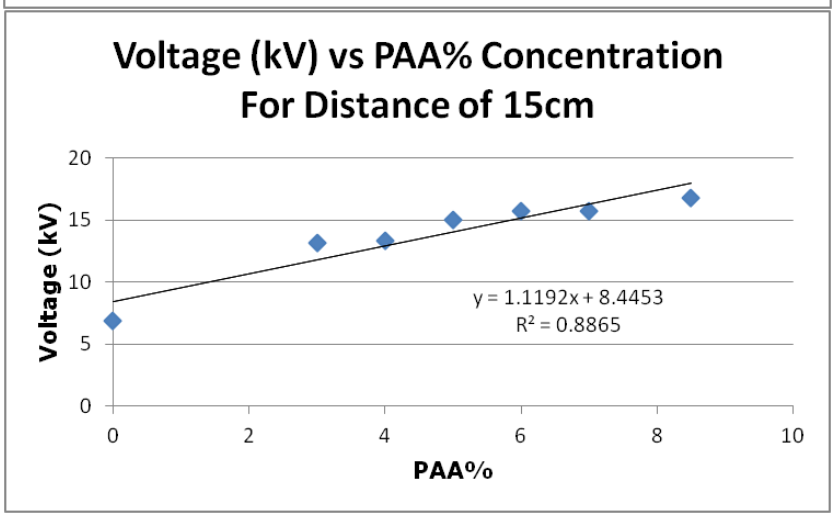

Figure 13: Shows the calculated Voltage (kV) for a specific distance, which takes into account the contact angle measured with solutions with different PAA% concentrations on Stainless Steel 316B L samples.

Electrospinning

When using the electrospinning equation, these were the measurements taken from the flat-tipped needle used to spin the scaffold run:

- R = 0.026cm
- L = 3.81cm

The electrospinning equation was simplified using the above variables:

$$V_C^2 = \frac{4 * H^2 * [4.18] * (\ 3.042 * 10^{-3} cm * \pi * \curlyvee)}{14.52 cm^2}$$

$$V_C^2 = \frac{0.051 cm * H^2 * (\ \pi * \curlyvee)}{14.52 cm^2}$$

$$V_C^2 = (\ 3.5 * 10^{-3}\ ) * H^2\ * (\ \pi * \curlyvee\ ) * cm^{-1}$$

SEM Images:

Pre Cross linked Fibers

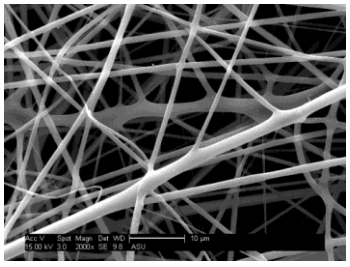

7%PAA-9cm-9.4kV

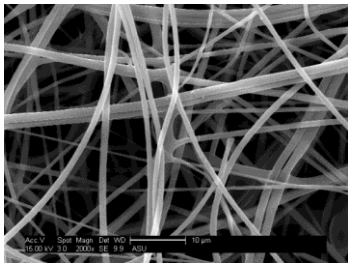

7%PAA-12cm-12.4kV

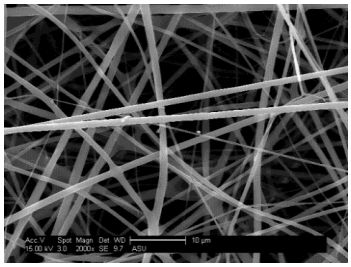

7%PAA-15cm-15.6kV

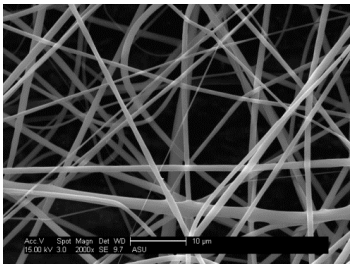

8.5%PAA-9cm-10.1kV

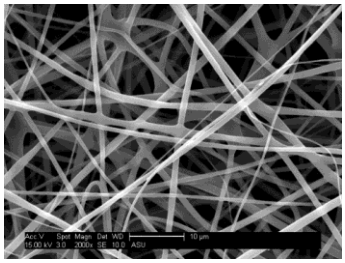

8.5%PAA-12cm-13.4kV

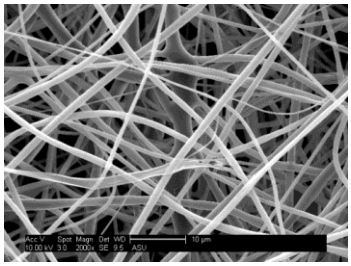

8.5%PAA-15cm-16.8kV

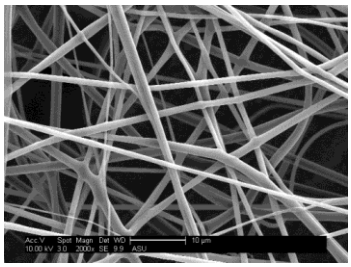

10%PAA-9cm-11.5kV

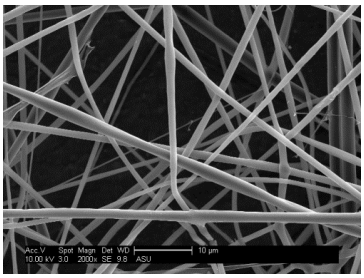

10%PAA-12cm-15.4kV

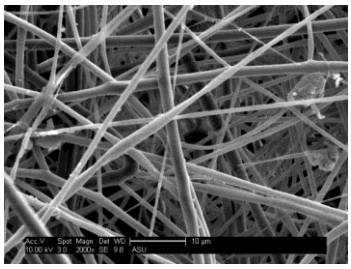

10%PAA-15cm-19.6kV

Figure 14: Shows the SEM images taken for all the pre-cross linked fibers for the scaffold runs.

Cross Linked Fibers

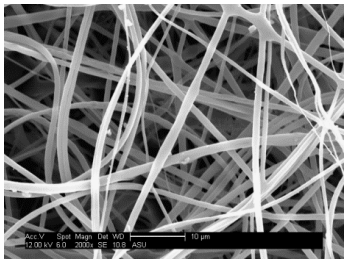

7%PAA-9cm-9.4kV

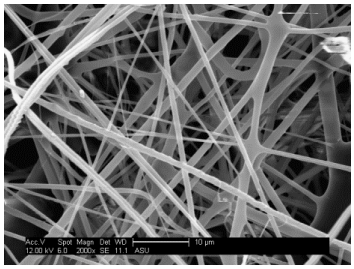

7%PAA-12cm-12.4kV

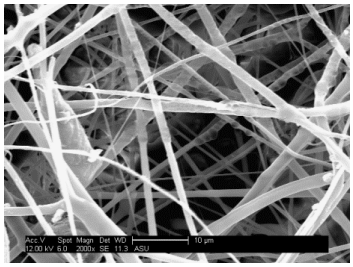

7%PAA-15cm-15.6kV

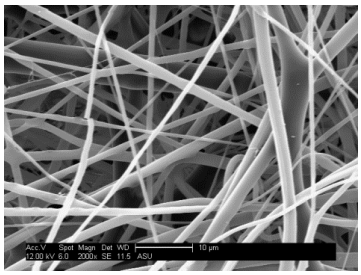

8.5%PAA-9cm-10.1kV

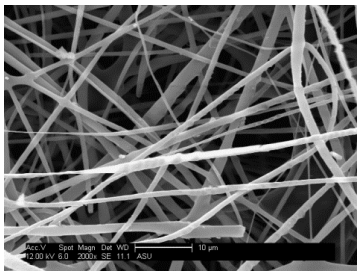

8.5%PAA-12cm-13.4kV

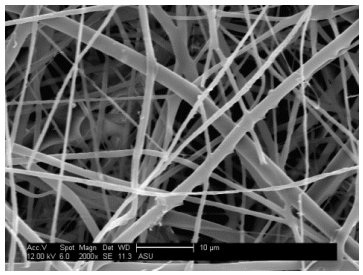

8.5%PAA-15cm-16.8kV

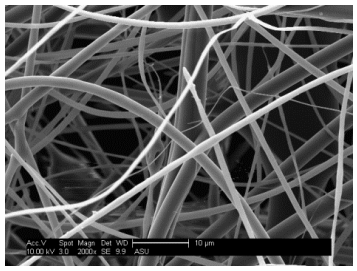

10%PAA-9cm-11.5kV

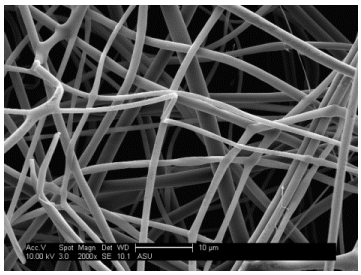

10%PAA-12cm-15.4kV

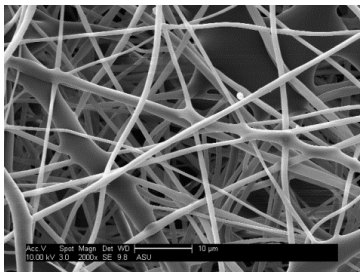

10%PAA-15cm-19.6kV

Figure 15: Shows the SEM images taken for the cross linked fiber of all the scaffold runs.

ImageJ Analysis:

Using ImageJ the fibers diameter and pore diameters of each SEM image were analyzed. Since the depth of the image cannot be determined from the SEM imaging, only the surface fibers were chosen for fiber and pore diameter analysis as shown in Figure 16 below.

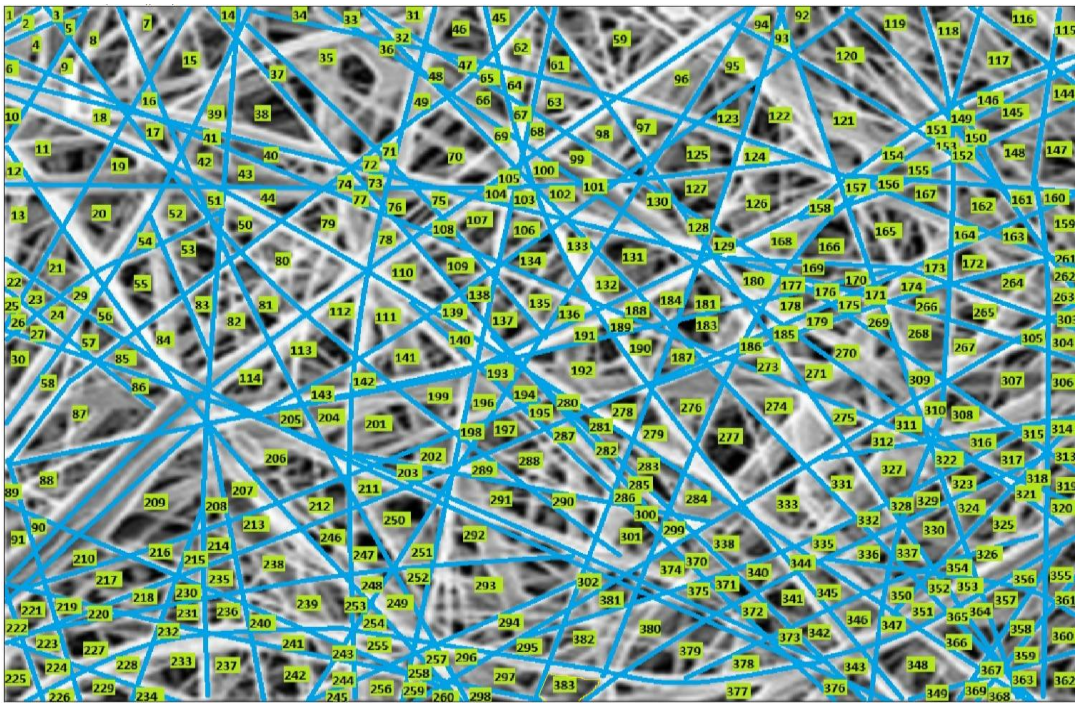

Figure 16: Shows the drawn surface fibers along with the pores (numbered) that were analyzed in imageJ.

Fiber Diameters (Pre-Crosslinked)

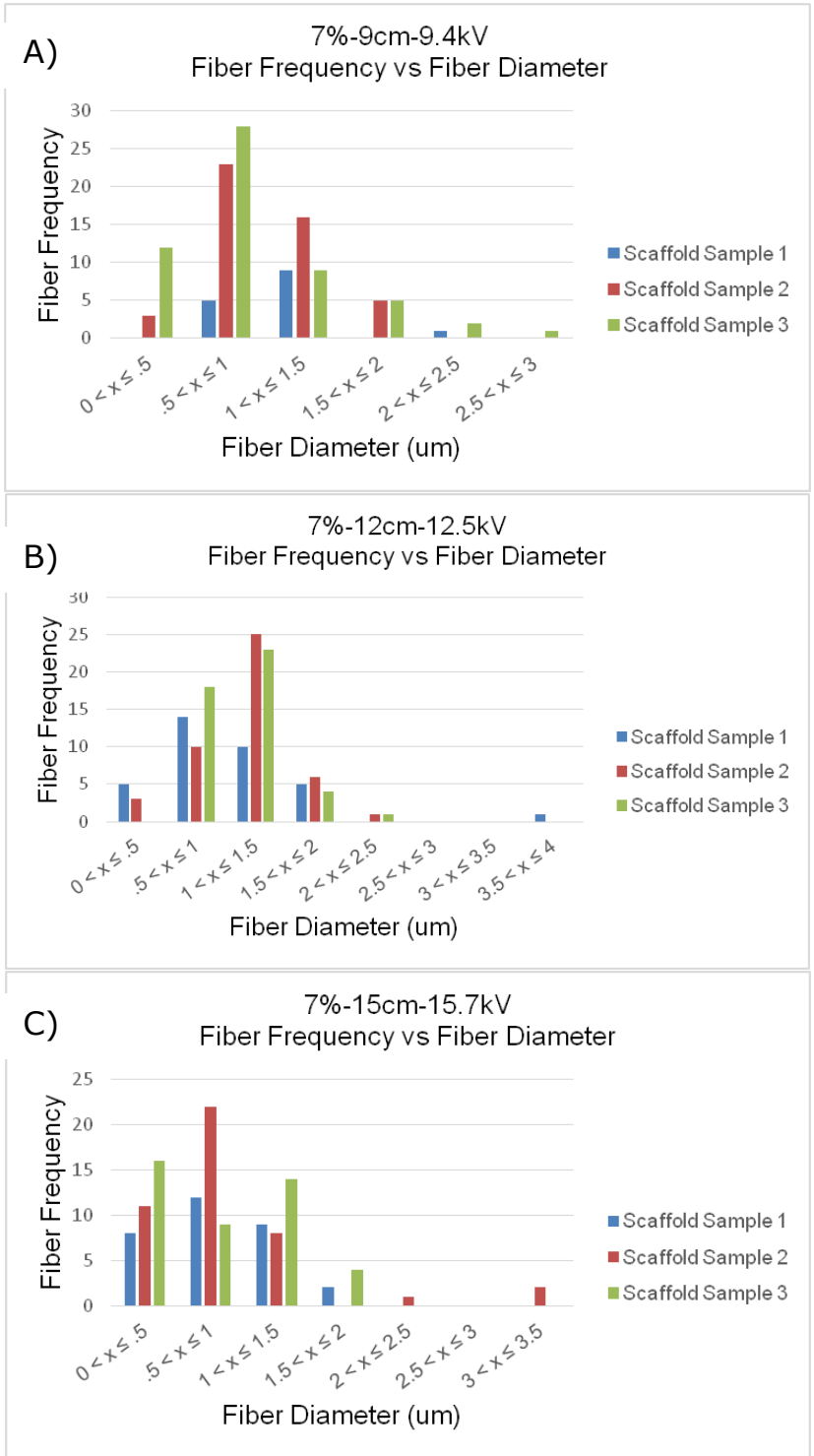

Figure 17 A-C: Shows Pre-Cross Linked fiber diameters and their frequency measured in the SEM images taken from 7%PAA concentrated scaffolds.

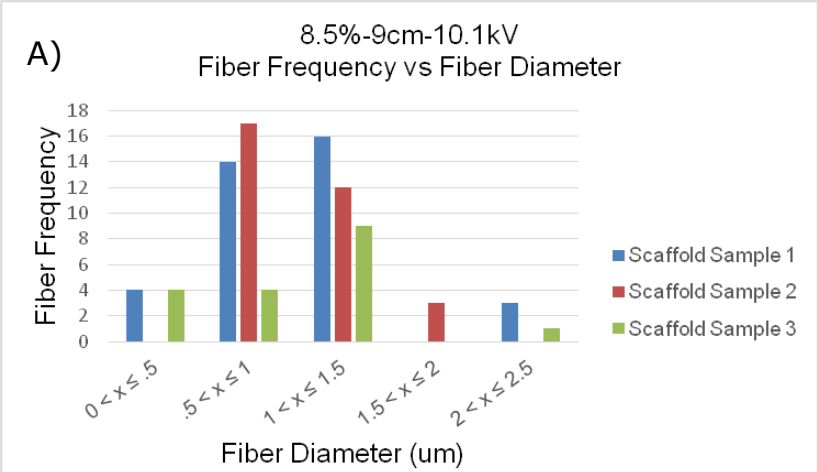

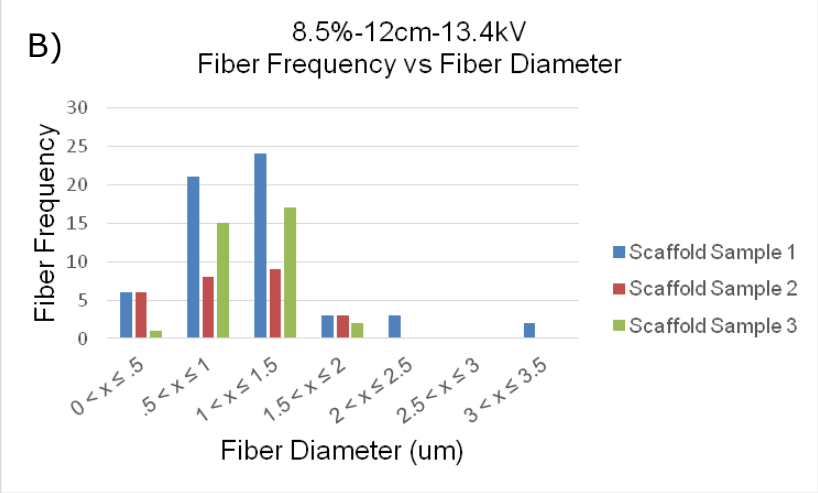

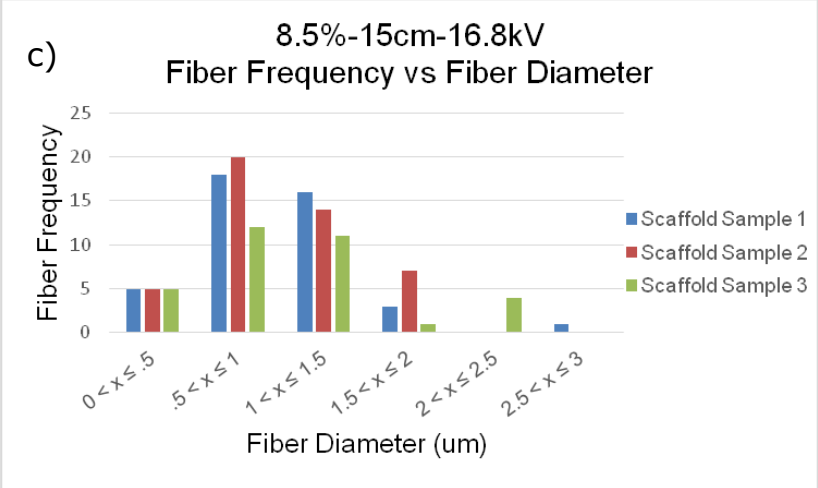

Figure 18 A-C: Shows Pre-Cross Linked fiber diameters and their frequency measured in the SEM images taken from 8.5%PAA concentrated scaffolds.

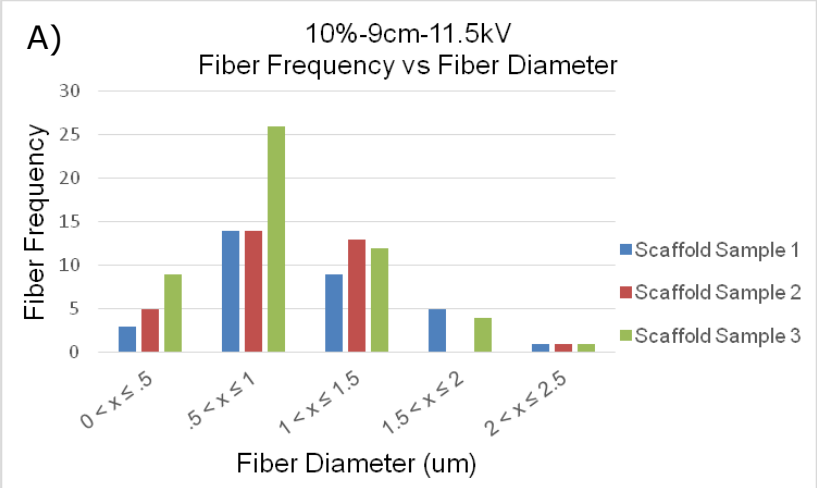

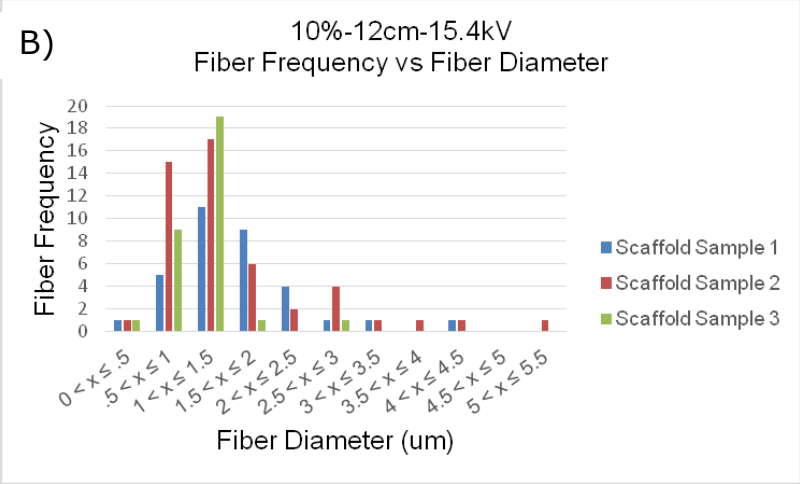

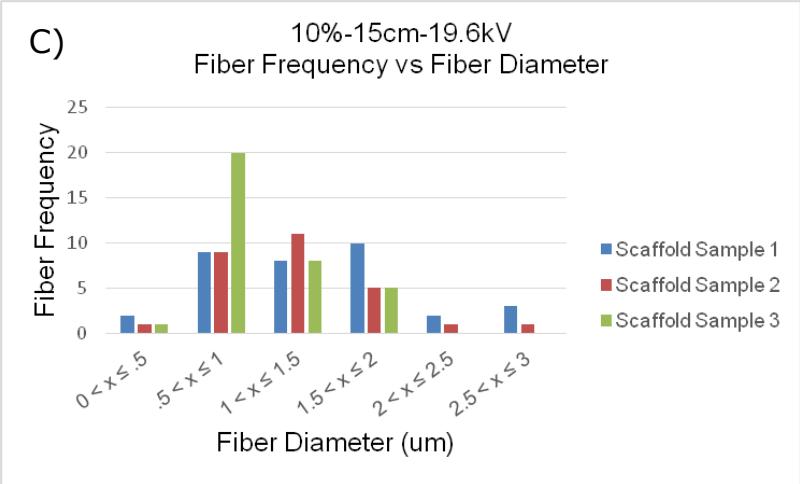

Figure 19 A-C: Shows Pre-Cross Linked fiber diameters and their frequency measured in the SEM images taken from 10%PAA concentrated scaffolds.

Pore Diameters (Pre Crosslinked)

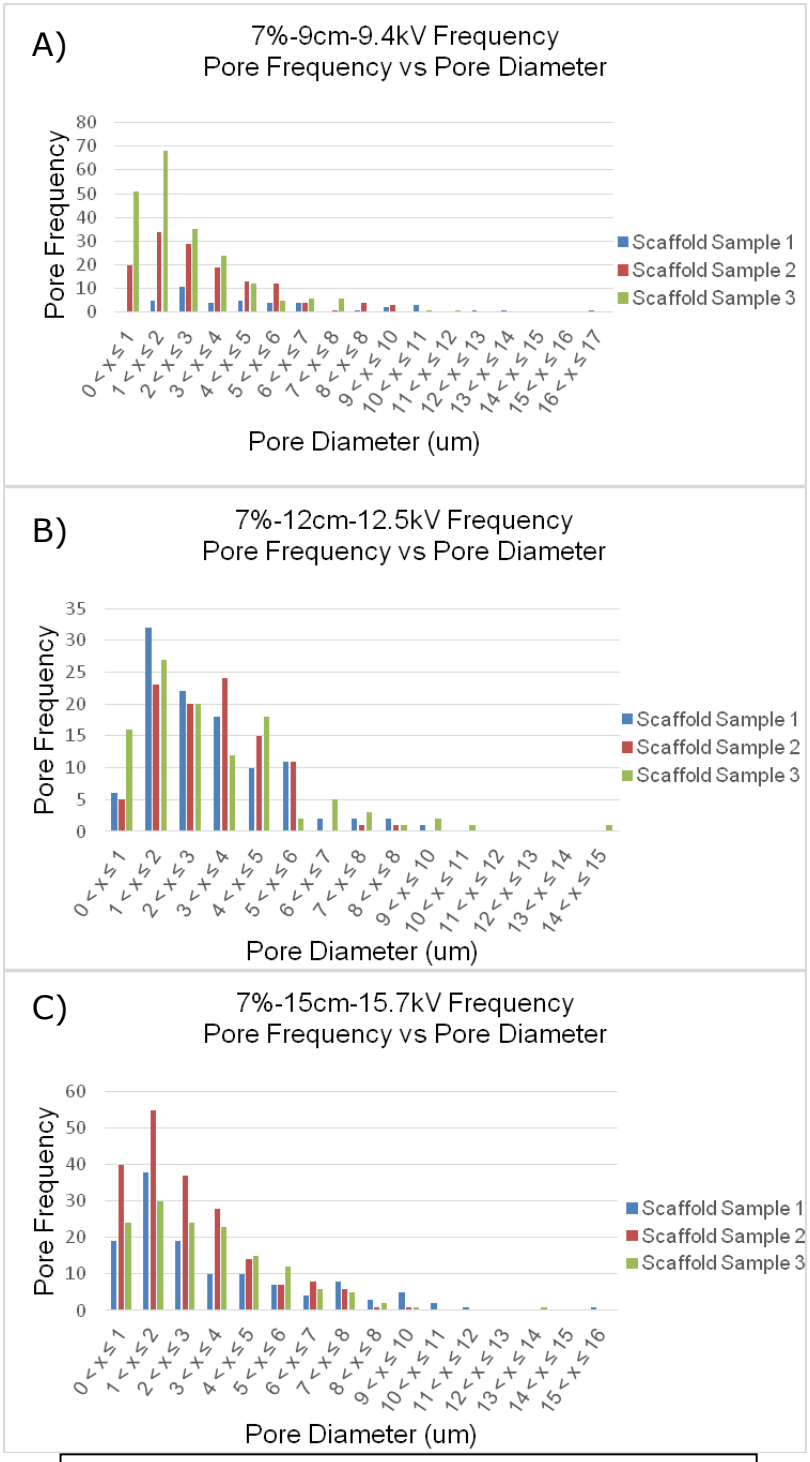

Figure 20 A-C: Shows Pre-Cross Linked fiber diameters and their frequency measured in the SEM images taken from 7%PAA concentrated scaffolds.

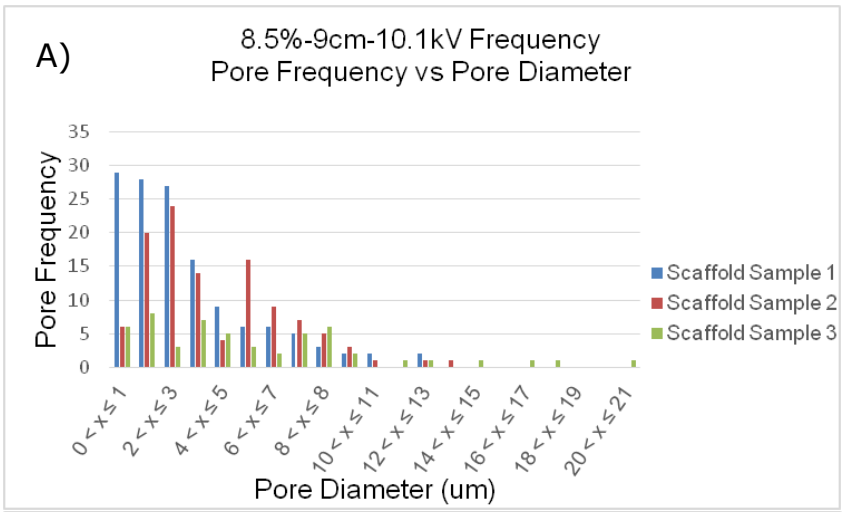

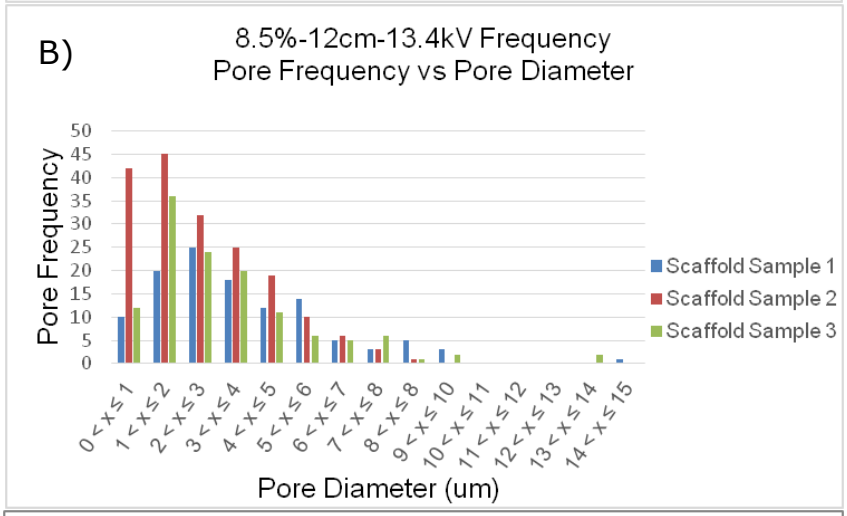

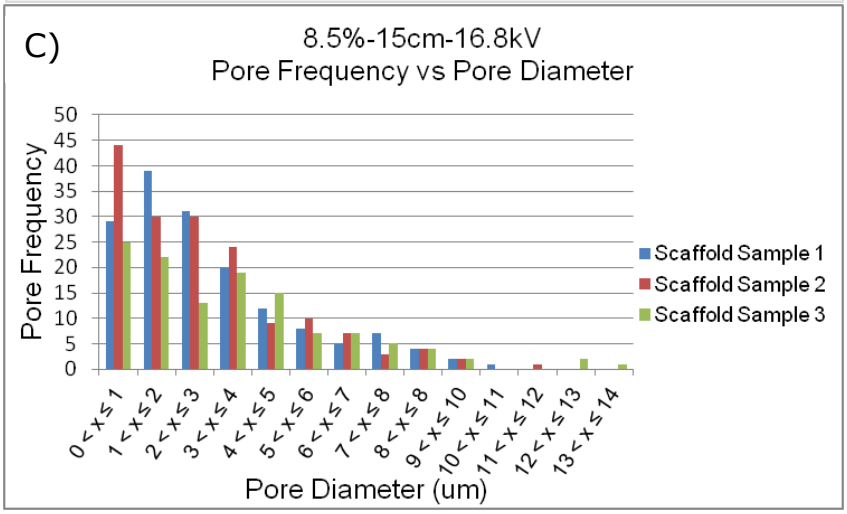

Figure 21 A-C: Shows Pre-Cross Linked fiber diameters and their frequency measured in the SEM images taken from 8.5%PAA concentrated scaffolds.

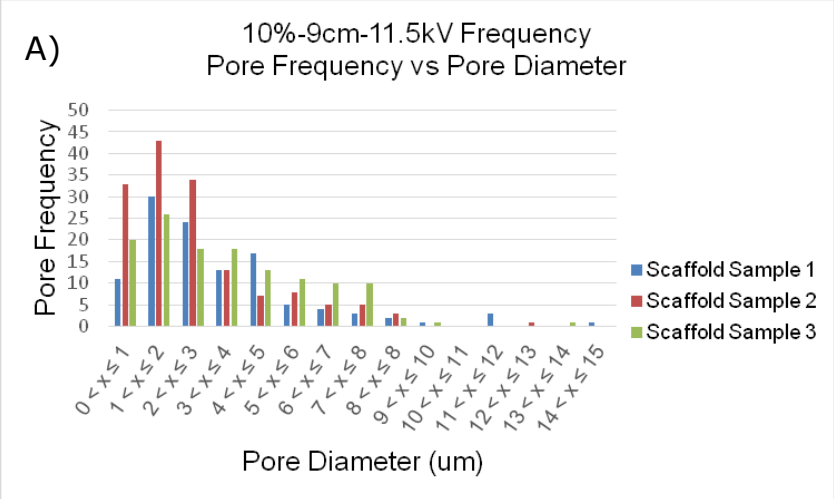

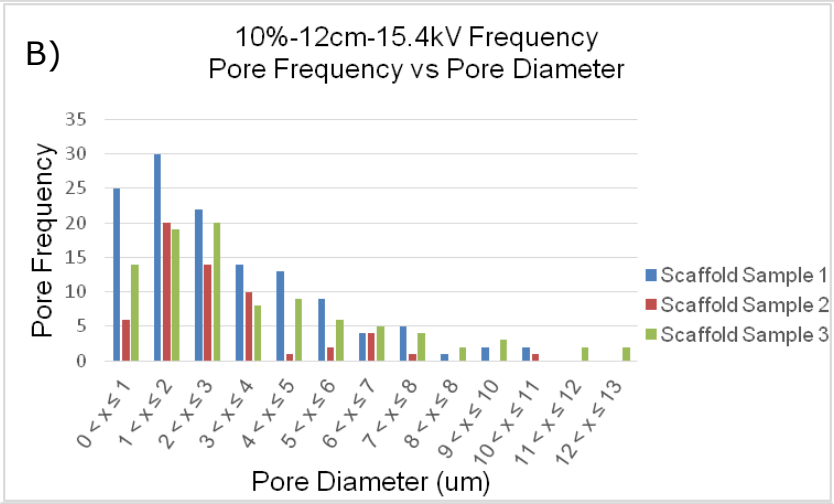

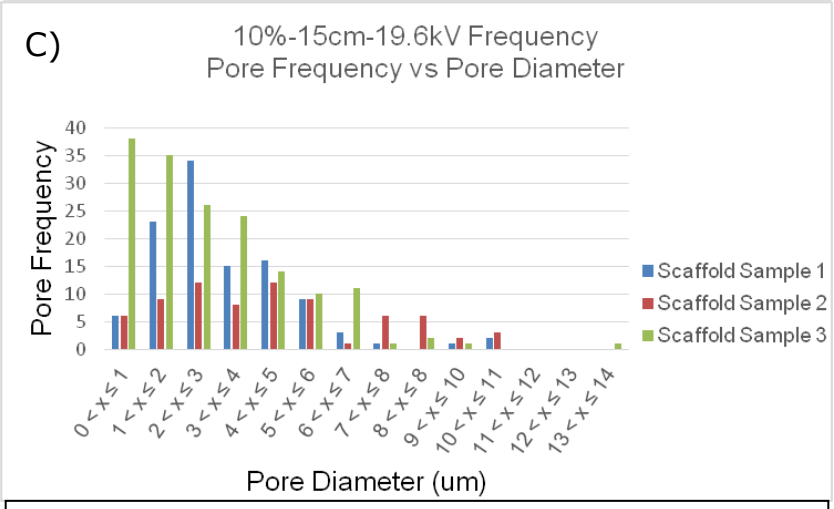

Figure 22 A-C: Shows Pre-Cross Linked fiber diameters and their frequency measured in the SEM images taken from 10%PAA concentrated scaffolds.

Fiber Diameters (Crosslinked)

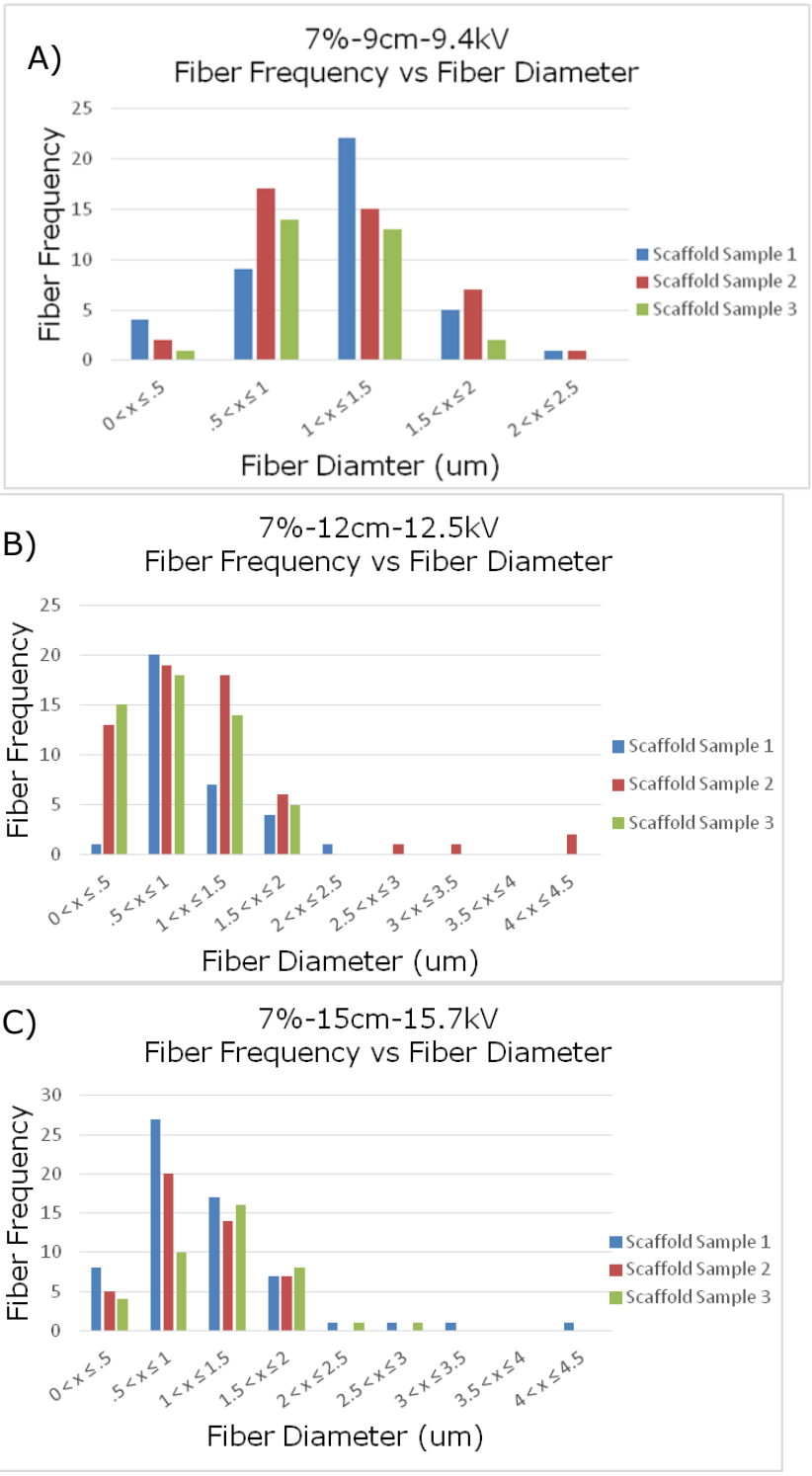

Figure 23 A-C: Shows cross-linked fiber diameters and their frequency measured in the SEM images taken from 7%PAA concentrated scaffolds.

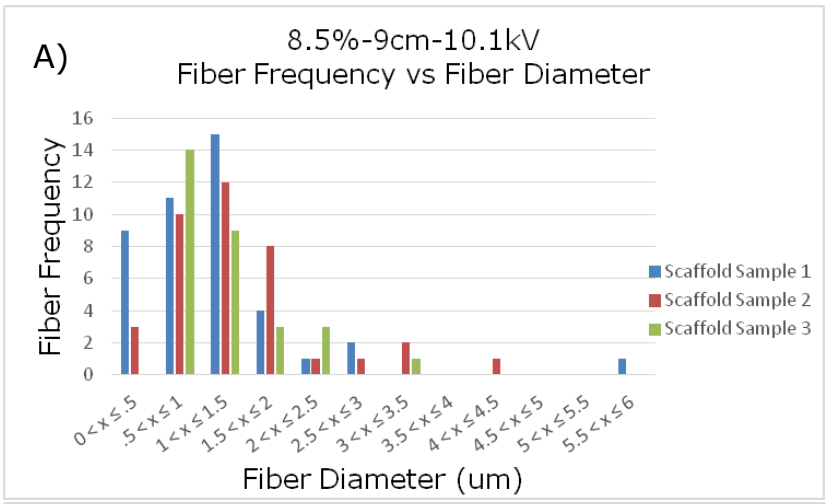

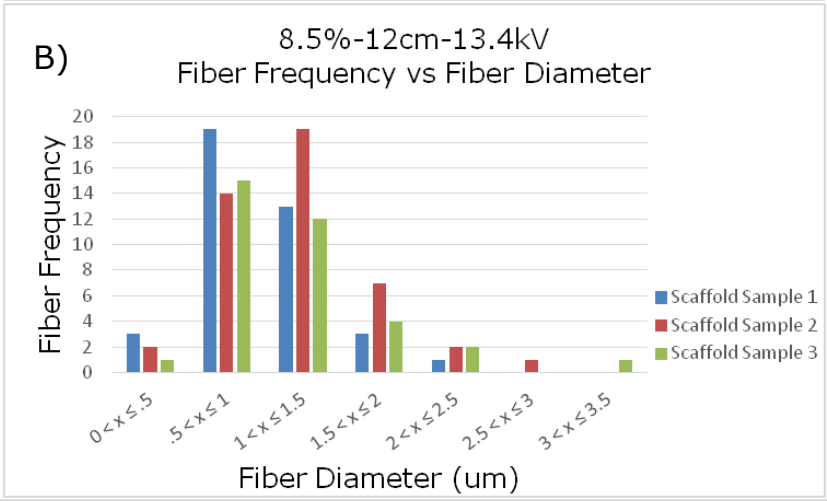

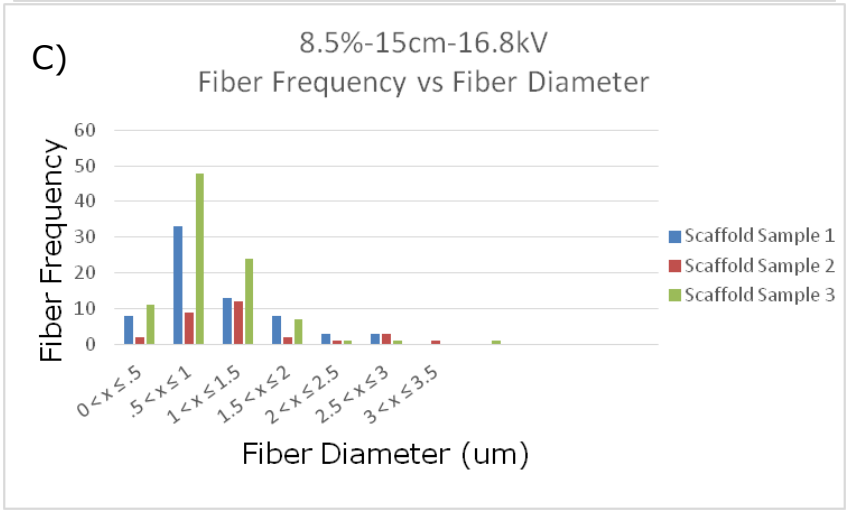

Figure 24 A-C: Shows cross-linked fiber diameters and their frequency measured in the SEM images taken from 7%PAA concentrated scaffolds.

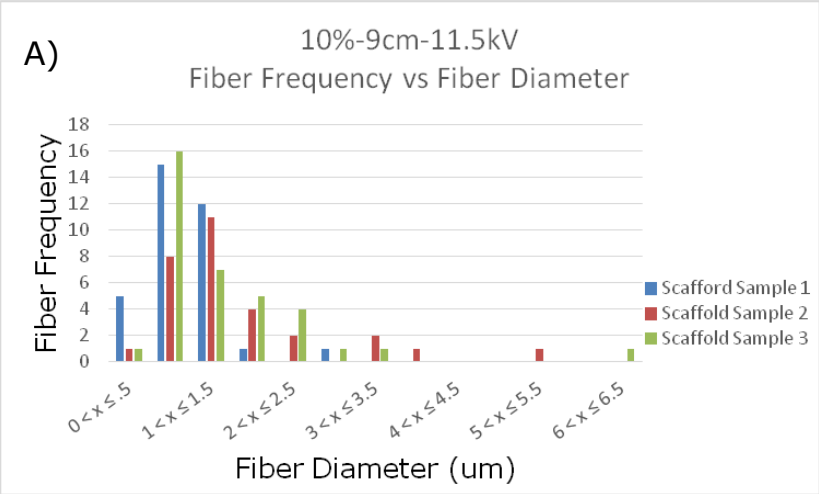

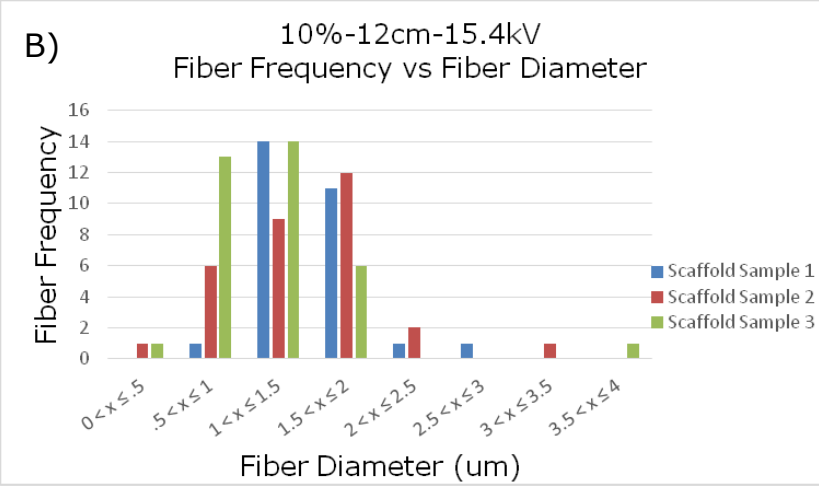

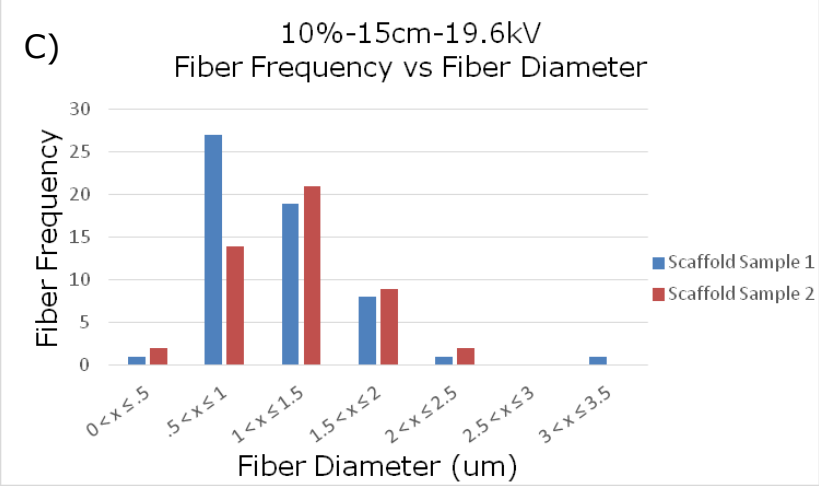

Figure 25 A-C: Shows cross-linked fiber diameters and their frequency measured in the SEM images taken from 10%PAA concentrated scaffolds.

Pore Diameters (Crosslinked)

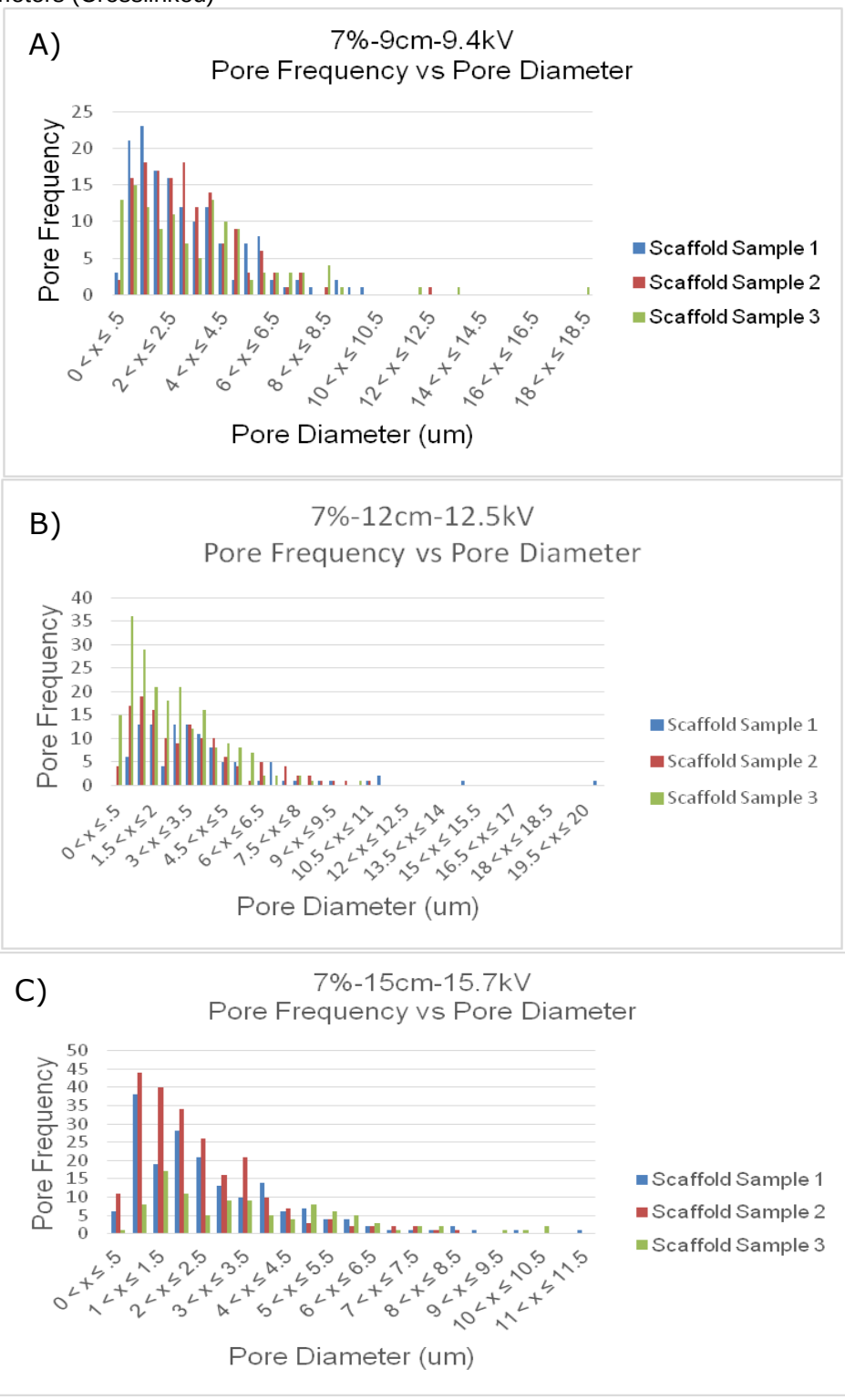

Figure 26 A-C: Shows cross-linked fibers and the pore frequency vs the pore diameter for a scaffold with PAA concentration of 7% and a Dextran wt% of 40%. The fibers were spun at three different distances.

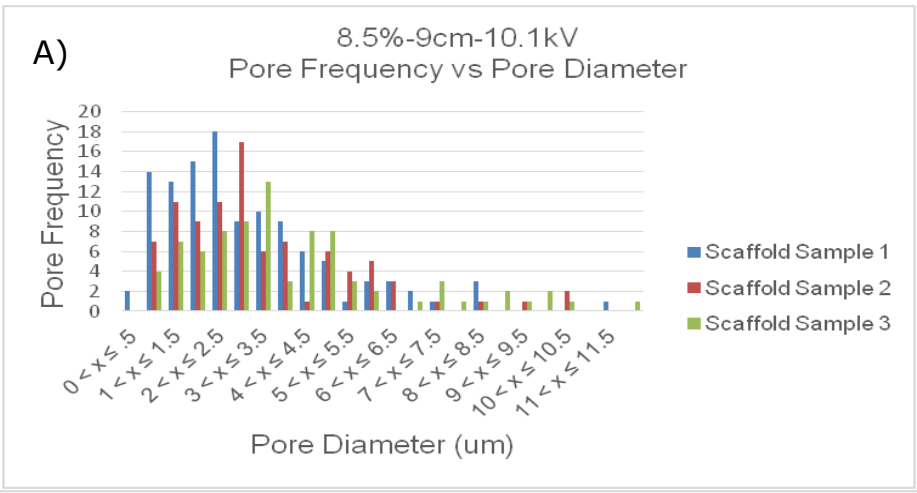

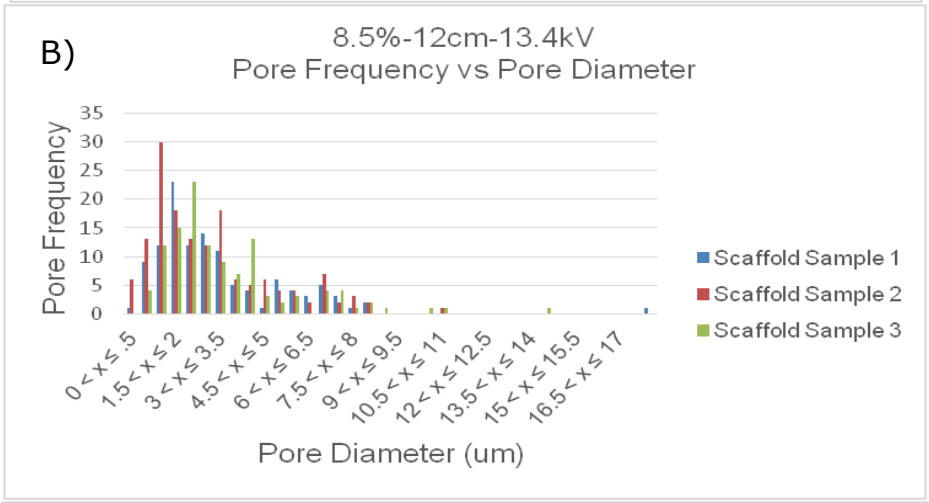

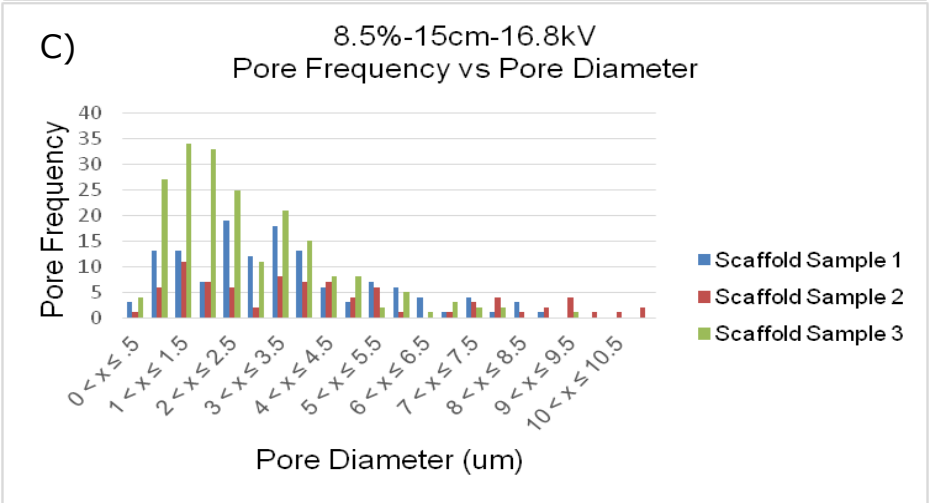

Figure 27 A-C: Shows the cross-linked fibers and the pore frequency vs the pore diameter for a scaffold with PAA concentration of 8.5% and a Dextran wt% of 40%. The fibers were spun at three different distances.

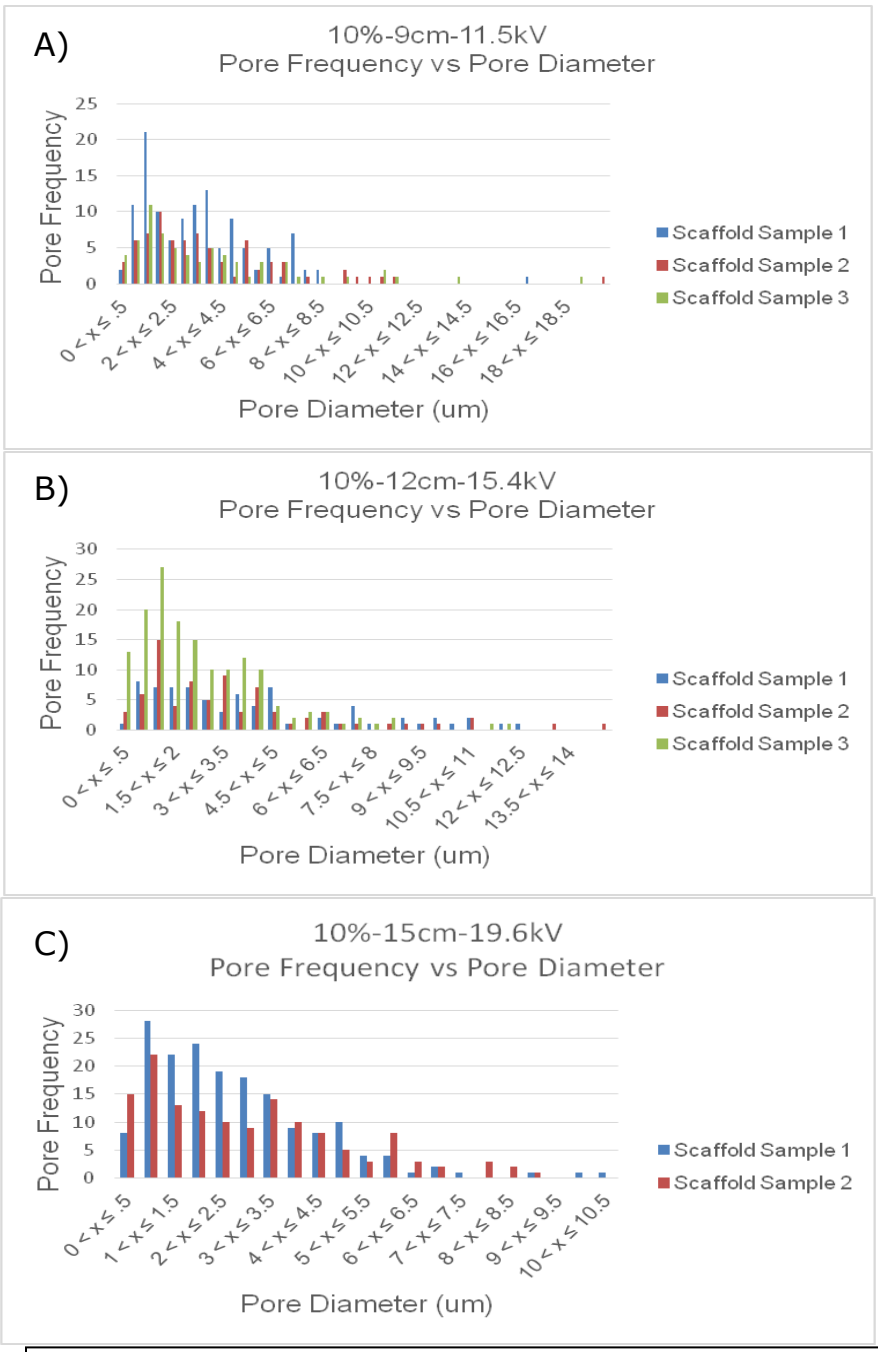

Figure 28 A-C: Shows the cross-linked fibers and the pore frequency vs the pore diameter for a scaffold with PAA concentration of 10% and a Dextran wt% of 40%. The fibers were spun at three different distances.

Porosity Data

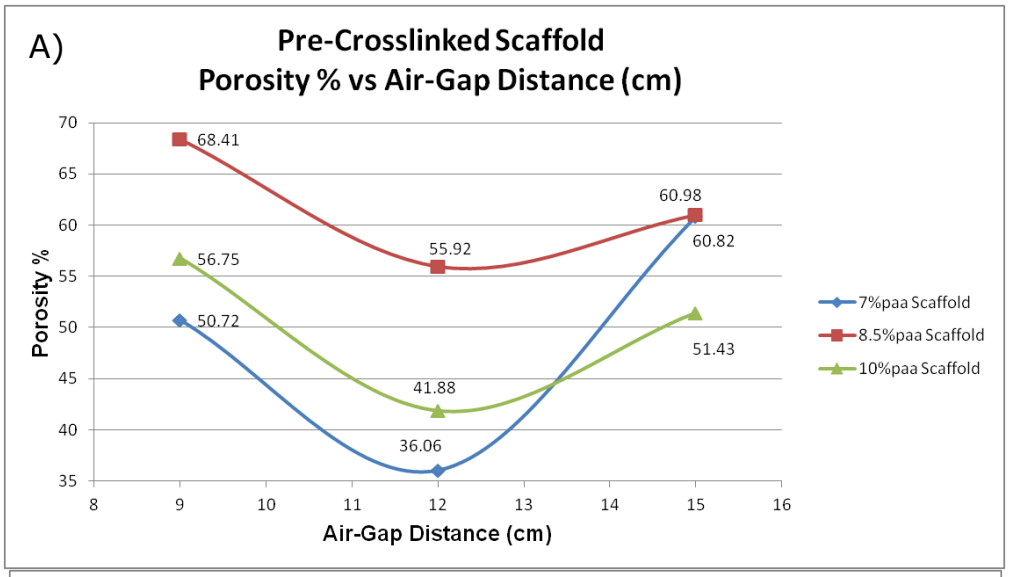

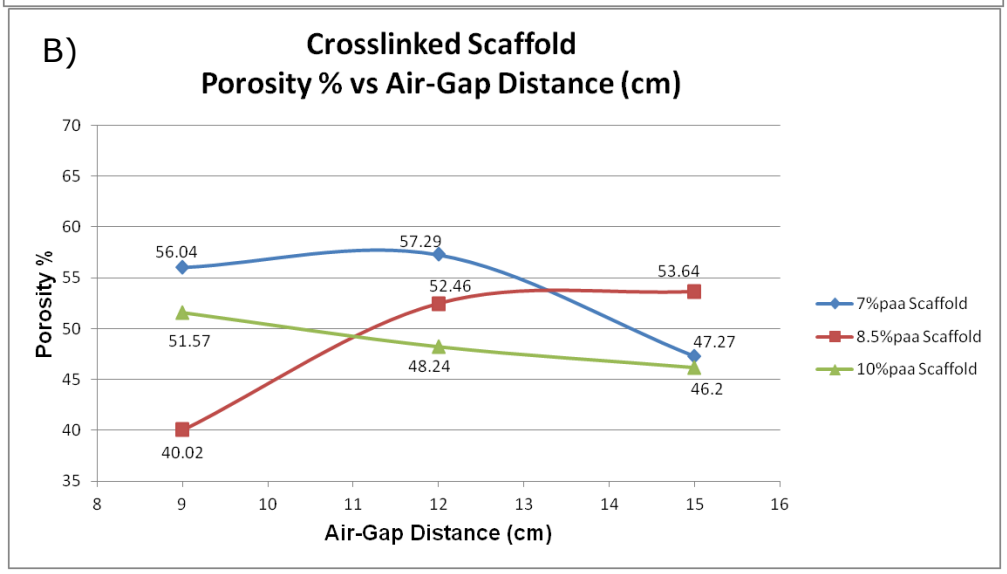

Figure 29 A-B: Shows the porosity % vs the air-gap distance (cm) for the scaffold range of paa concentration with a range of distance.

Contour Maps

Pre-Crosslinked Data

A)

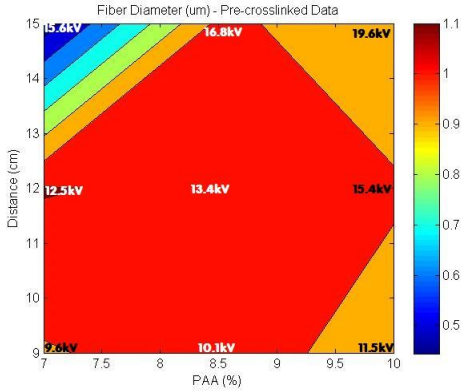

B)

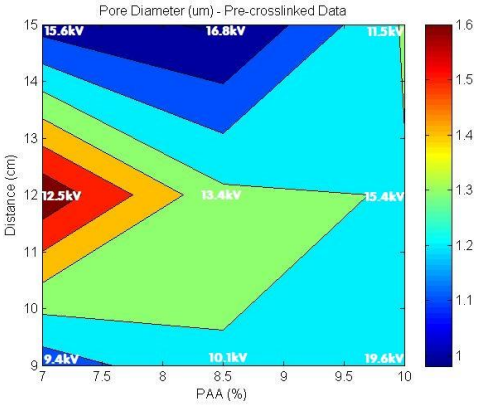

C)

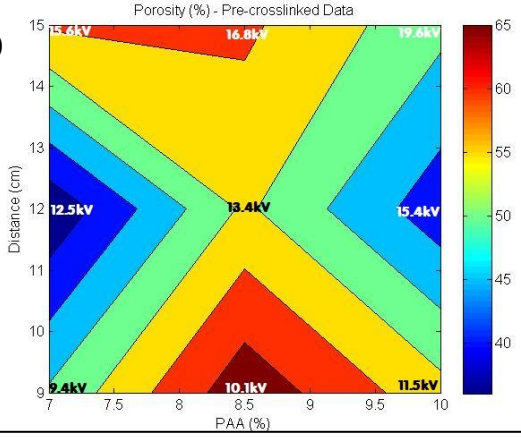

Figure 30 A-C: Shows the counter map of the Air-Gap Distance Vs the Concentration 40wt% Dextran with varying PAA%. The scale bar at the right hand side shows the unit range of the dependent variable stated in the title. The Voltage used to electrospin was stated throughout the map.

Cross-linked Data

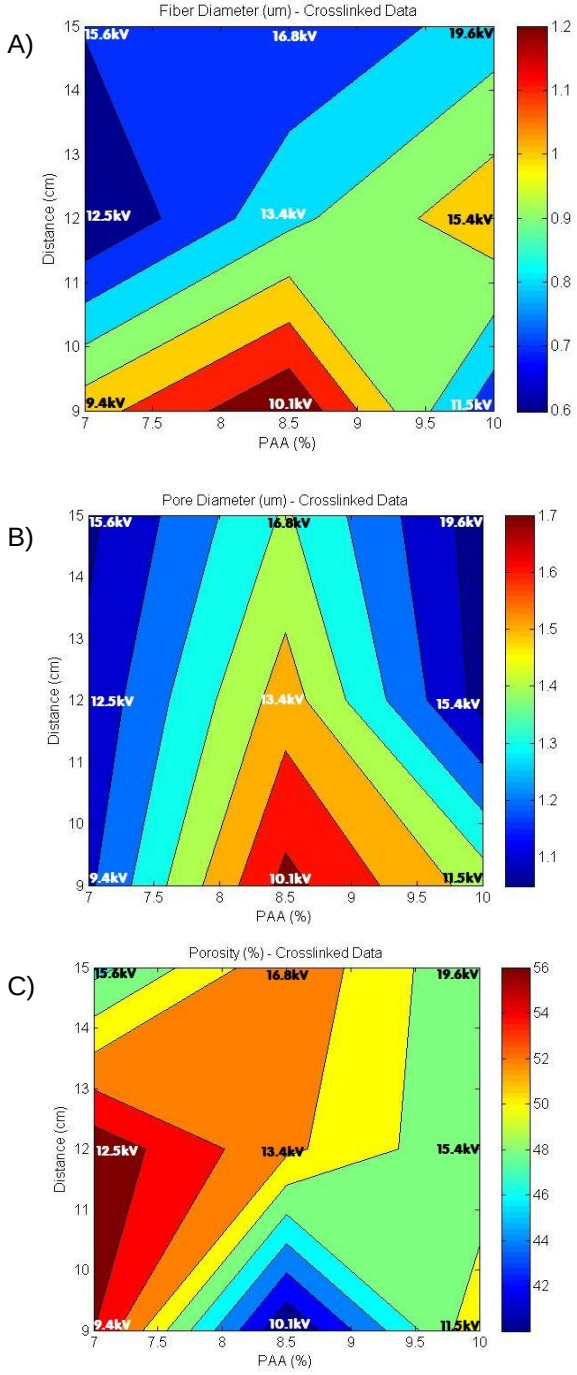

Figure 31 A-C: Shows the counter map of the Air-Gap Distance Vs the Concentration 40wt% Dextran with varying PAA%. The scale bar at the right hand side shows the unit range of the dependent variable stated in the title. The Voltage used to electrospin was stated throughout the map.

CHAPTER 5

DISCUSSION

The project objectives were to determine the electrospinning operating conditions of the process variables that would lead to desired Dex-PAA scaffold structures. Understanding the interactions between the variables in equation 3 allows the user to be able to control their system to a high degree. The overall goal was to determine how the independent variables from equation 3 would affect the dependant variables of fiber diameter, pore sizes, fiber orientation, and mechanical properties.

Fiber diameter and pore sizes remain as one of the most important factors determining the functionality of the scaffold, as the pore sizes will ultimately set the ranges of porosity throughout the system creating the area-to-volume ratios that would directly affect the way the cells would interact with their environments and produce the needed amount of connective tissue at a timely rate. Pore symmetry, or the path of the pores through the structure, also influences cellular migration throughout the scaffold structure.

Preliminary Literature Review of Electrospun Scaffold Systems

A careful investigation in the design of nanoscale electrospun synthetic scaffolds was done by conducting a comprehensive literature search on the design, fabrication, characterization, and in vitro evaluation and a preliminary analysis of reported findings pertaining to electrospun scaffolds. It is believed that a more systematic approach regarding the design rational of nanoscale fiber constructs would be of great benefit. This study proposed to take a more global design approach that considers the following key variables and their interactions. These include fiber composition, diameter, and orientation, as well as scaffold pore-size, porosity, and geometry. Also the composite nature of the scaffold, scaffold mechanical properties, as well as the surface area, and surface energy the scaffold offers.

Examples of scaffold polymer materials that can be electrospun are; Polycaprolactone (PCL), poly(lactic-co-glycolic acid) (PLGA), poly(L-lactic acid) (PLLA), and poly(3-hydroxybutyrate-co-3-hydroxyvalerate) (PHBV). In addition nanoparticles such as hydroxyapatite (HA) or carbon nanotubes can be utilized for designated electrospun scaffold constructs. The

mechanical properties of the fibers can also be determined by measuring the tensile strength, ultimate strain, which can be utilized in a stress-strain curve to determine the stiffness of the fibers.

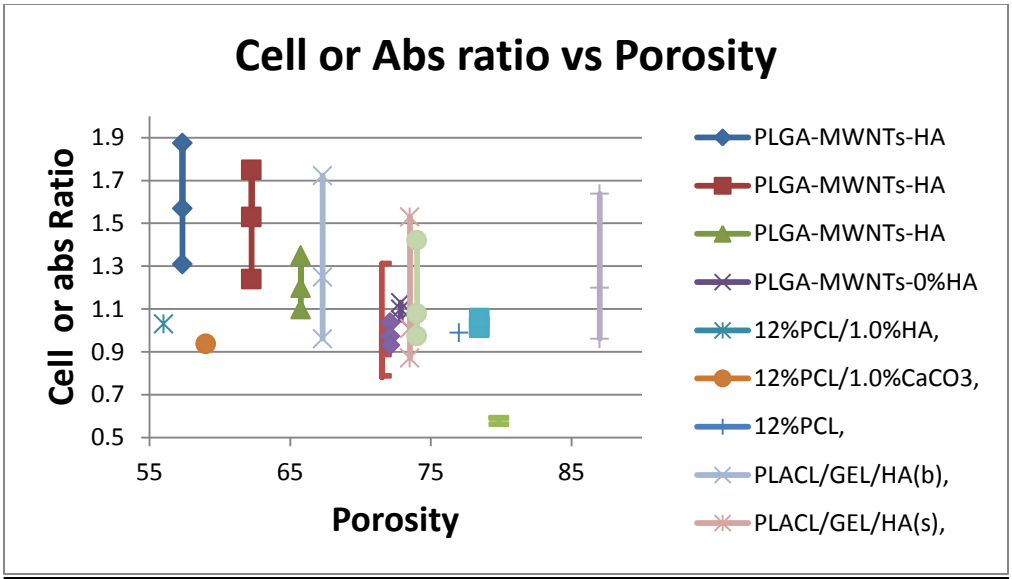

Figure 32: Shows the normalization of cellular absorbance ratio or cell count ratio vs the porosity of the scaffolds from the literature review of all the journal articles from table 1 [16, 22, 25, 33, 51].

Using the program ImageJ, the porosity of scaffolds were measured from the SEM images given in the articles. Figure 32 shows the normalization of cellular absorbance ratio or cell count ratio vs the measured porosity of the scaffold images. The plot shows that the highest cellular levels were around mid fifty percent scaffold porosity, however the measured data stopped at the mid fifty range, it leaves questions to whether a lower porosity range is capable of encouraging higher cellular proliferation. Figure 32 also shows that cellular levels begin to rise a second time around the high eighty percent, porosity range which suggest that other scaffold porosity values, yet to be confirmed, may exist where cells may best proliferate.

Preliminary Scoping of Electrospinning Dex-PAA

A preliminary run on electrospinning the Dex-PAA system was done in order to understand the conditions that suited this solution system during electrospinning. As shown in figure 9 in the experimental section, the area in which electrospinning was observed with minimal beading was mapped out. Having found from the literature review that beading would decrease

the functionality of the scaffolds and deem them defective in both mechanical and structural aspects of mimicking the tissue ECM structures. The electrospinning equation was taken into account when running the prelimnary scope, as the variables deemed by literature to be most detrimental in changing the ranges of fiber diameters and porosity, would be voltage (kV) and distance (cm). Literature suggested that the limits of the variables should be set from 15-25kV and 9-15cm in order to produce reliable spinning conditions for consistent desired outputs and structural integrity of the fibers. The solution concentration for PAA was kept constant at 8.4v/v% with a Dextran concentration of 40wt%. Two Dextran molecular weights were tested at 70kD and 500kD, the data for the 70kD can be found in the appendix. On all three distances tested, functional electrospinning occurred around 15kV-25kV. Beading was still observed, and in specific electrospinning conditions the beadings were either minimal or counterproductive to the process.

Once an understanding was obtained as to what the processing conditions look like for the polymer system studied herein, a step back was taken to understand the electrospinning equation and it was determined that optimizing the variable ranges for electrospinning could rely on the surface tension variable that went untested in the preliminary scope.

Surface Tension of the Electrospun Dex-PAA Solutions

The electrospinning equation includes a variable that takes into consideration the surface tension (Y) of the solutions being electrospun. In order to refine the equation and optimize the electrospinning parameters, the surface tension of the Dex-PAA solutions were measured on the same material type that the syringe needle was made up of, Stainless Steel 316B L. The contact angles measured on the stainless steel flat surface samples were done using several solution mixtures of Dex-PAA. The Dextran concentration was kept at 40wt%, while the PAA concentration was kept at 3-8.5v/v%. Higher concentrations of PAAv/v% were difficult to measure on the goniometer, which led to using a lower range of concentrations.

Electrospun Scaffolds

To create fibers in the nano-scale to micro-scale range, selected process variables were modified: PAA solution concentration and distance (cm). SEM images of electrospun fibers were analyzed to measure the fiber diameter and overall morphology such as fiber frequency and fiber angles.

Pre-Cross Linked Scaffolds

The effects of varying PAA polymer concentration showed that higher PAA concentrations produce higher fiber diameters. The fiber diameter range spun in the 7-10% PAA range showed diameters of 0.1-5um, as shown in figures 17-19. The lower PAA% concentrations showed higher frequency of fiber diameters below the 1um range. The 10% PAA solution gave the highest fiber diameters at around 5um. Spinning the 7, 8.5, and 10% PAA solutions concentrations at different distances of 9, 12, and 15cm showed the fiber diameter get smaller the further the collecting target was away for all concentrations. The lower concentrations showed that the fibers can be stretched more easily the further it spun from the target.

Pore Diameters

The pore diameters (shown in figures 20-22) showed, on average, across all concentrations to be around 0-4um. The diameters of the pores ranged from less than a micro-meter to as large as 18um in some cases. The largest pore diameters were found when the PAA concentration was at 8.5%, from there the diameters seemed to decrease a bit when spinning PAA at 7% or 10%. Though it was also found that the lower concentrations of PAA spun, gave a higher frequency of smaller pore diameters.

Crosslinked Scaffold

Crosslinking the scaffolds produced a higher frequency of higher fiber diameters, shown in figures 23-25. The 7%paa showed an increase in fiber diameter range of 1-2um, and as the concentration increased to 8.5%paa the fiber diameter range is seen to double, but still maintained the average of fiber diameters in the 0.5-2um range. At 10%paa, the effects of

crosslinking was evident with the lower and higher ranges of paa% concentration showing fiber diameter reaching around 6-6.5um for an air-gap distance of 9cm, while the uncrosslinked fiber diameter for those same parameters reached only around 2-2.5um. The pore diameters, shown in figures 26-28, stays around the same range of 0-8um for both pre-crosslinked and crosslinked scaffolds, but lower frequency of the pore are found in the thermally crosslinked scaffolds. This indicates that the fibers are clearly melting and morphing their fibers. A decrease in pore size is apparent across all concentrations of paa%.

Scaffold Porosity

Finally, the porosity has a wider range for scaffolds that were pre-crosslinked when compared to the crosslinked scaffolds as shown in figure 29. In fact the pre-crosslinked scaffolds showed a porosity range of 36-68%, while crosslinking the scaffolds produced a porosity range of only 40-56%. The lower porosities were found under the pre-crosslinked scaffold of 7%paa. The 10%paa concentration did produce a porosity range of around 42%, close to the 7%paa concentration, but when electro spun at 8.5%paa the porosity shot up to low 56% and high 68%, depending on the air-gap distance.

CHAPTER 5

CONCLUSION

A wide variety of fiber morphology can be produced with the Dex-PAA scaffolds having a wide range of fiber diameters and pore diameters. By changing two of the electrospun process variables, i.e., PAA concentration and air-gap distance, the diameter ranges can be altered to desired outputs when considering mimicking the ECM through electrospinning, as shown in figures 30-31. Further work would continue in conducting a full L9 DOE factorial, focusing on testing a range of Voltage (kV) for a range of air-gap distances (cm). Finally, the addition of carbon nanotubes to the Dex-PAA , would affect scaffold mechanical properties, e.g., tensile strength, and architecture which would possibly enhance cellular proliferation. If so, optimization of process parameters would be warranted, taking similar approaches than that taken in this study to optimize electrospinning process conditions, as solution conductivity changes from the addition of the carbon nano-tubes would likely alter electrospinning process conditions.

REFERENCES

[1] Broderick N. 2009, Understanding chronic wound healing, *The American Journal of Primary Health Care*, 34: 16-22

[2] Buxton RS and Magee AI 1992, Structure and interactions of desmosomal and other cadherins, *Semin Cell Biol*, 3: 157-67

[3] Cai Xing Z, Jin Han S, Suk Shin Y, Kyu Kang I. 2011, Fabrication of Biodegradable Polyester Nanocomposites by Elecrospinning for Tissue Engineering, *J Nanomater*, 2011: 18 pages

[4] Chen X, Zhu N. 2013, Biofabrication of Tissue Scaffolds, Univesity of Saskatchewan, Saskatoon, SK, Canada.

[5] Chesini IM. Substrates and ligands of the protein tyrosine phosphatase ptprr in neuronal cell signaling, Friedrich Shiller University, Jena, Verona, Italy.

[6] Chibowski S and Paszkiewicz M 2006, Polyacrilic Acid (PAA) Adsorption on Alumina (Al_2O_3) Surface. Influence of Sodium Dodecyl Sulfide (SDS) on Adsorption in PAA-SDS- Al_2O_3 System, *Physiocehm Probl Mi*, 40: 175-184

[7] Coles SR, Jacobs DK, Meredith JO, Barker G. 2009, A Design of Experiments (DoE) Approach to Material Properties Optimization of Electrospun Nanofibers, *J Appl Polymer Science*, 117: 2251-2257

[8] Cui W, Li X, Zhou S, Weng J. 2006, Investigation on Process Parameters of Electrospinning System through Orthogonal Experimental Design, *J Appl Polymer Science*, 103: 3105-3112

[9] Dai Z and Shivkumar S 2006, Electrospinning of hydroxyapatite fibrous mats, *Mater Lett*, 61: 2735-2738

[10] Davis GE and Senger DR 2005, Endothelial Extracellular Matrix: Biosynthesis, Remodeling, and Functions During Vascular Morphogenesis and Neovessel Stabilization, *Circ Res*, 25: 1093-107

[11] Bhola B, Nosovitskiy, Mahalingam H, Steier WH. 2009, Sol-Gel-Based Integrated Optical Microring Resonator Humidity Sensor, *IEEE Sensors J*, 9: 740-747

[12] Frantz C, Stewart KM, Weaver VM. 2010, The extracellular matrix at a glance, *J Cell Sci*, 123: 4195-4200

[13] Garcia AJ. 2005, Get a grip: integrins in cell-biomaterial interactions, *Biomaterials*, 26: 7525-7529

[14] Garg K, Bowlin GL. 2011, Electrospinning jets and nanofibrous structures, Biomicrofluidics, 5: 013403-1-013403-17

[15] Gu J, Isaji T, Xu Q, Kariya Y. 2012, Potential roles of N-glycosylation in cell adhesion, *Glycoconjugate J*, 29: 599-607

[16] Gupta D, Mitra JV. 2009, Nanostructred biocomposite substrates by electrospinning and electrospraying for the mineralization of osteoblasts, Biomaterials,30(11):2085-94

[17] Gu SY and Ren J 2005, Process Optimization and Empirical Modeling for Electrospun Poly (DmL-lactide) Fibers using Response Surface Methodology, *Macromol Mater Eng*, 290: 1097-1105

[18] Gumbiner BM. 1996, Cell Adhesion: The Molecular Basis of Tissue Architecture and Morphogenesis, *Cell Press*, 84: 345-357

[19] Harburger DS and Calderwood DA 2009, Integrin signaling at a glance, *J Cell Sci*, 122: 159-163

[20] Hoorfar M, Kurz MA, Policova Z. 2005, Do Polysaccharides Such as Dextran and Their Monomers Really Increase Tension of Water?, Langmuir, 22: 52-56

[21] Lai HC, Zhuang LF, Liu X, Wieland M, Zhang ZY. 2010, The influence of surface energy on early adherent events on osteoblast on titanium substrates, *J Biomed Mater Res A*, 93: 289-296

[22] Lao L, Wang Y, Zhu Y. 2011, Poly(lactide-co-glycolide)/hydroxyapatite nanofibrous scaffolds fabricated by electrospinning for bone tissue engineering, J Mater Sci, 22:1873-1884

[23] Li B and Wang JH 2011, Fibroblasts and myofibroblasts in wound healing: force generation and measurement, *J Tissue Viability*, 20: 108-120

[24]Li wj. 2002, Electrospun nanofibrous structure: A novel scaffold for tissue engineering. *Wiley Periodicals*. 60.4: 613-621

[25] Low S, Venugopal JR. 2008, Nanobioengineered electrospun composite nanofibers and osteoblasts for bone regeneration, International Center for Articial Organs and Transplantation and Blackwell Publishing, 32(5): 388-397

[26] Masutani G and Stenstrom MK 1984, A Review of Surface Tension Measuring Techniques, Surfactants, and Their Implications for Oxygen Transfer in Wastewater Treatment Plants.

[27] McAnulty RJ. 2007, Fibroblasts and myofibroblasts: their source, function and role in disease, *Into J Biochem Cell Biol*, 39: 666-671

[28] Mei F, Zhong J, Yang Z, Ouyang X. 2007, Improved Biological Characteristics of Poly(L-Lactic Acid) Electrospun Membrane by Incorporation of Multiwalled Carbon Nanotubes/Hydroxyapatite Nanoparticles, *Biomacromolecules*, 8: 3729-3735

[29] Ming Huang Z, Z Zhang Y, Kataki M, Ramakrishna S. 2003, A review on polymer nanofibers by electrospinning and their applications in nanocomposites, *Compos Sci Technol*, 63: 2223-2253

[30] Nature. 2000, Tissue Engineering. *Nature Biotechnology* . 18: IT56-IT58

[31] Niessen CM and Gumbiner BM 2002, Cadherin-mediated cell sorting not determined by binding or adhesion specificity, *Journal of Cell Biology*, 156: 389-400

[32] Pajic-Lijakovic I, Plavsic M. 2012, Influence of microenvironment on cell adhesion, polarization, and migration, International Journal of Nanomedicine, 7: 3473-3474

[33] Pavasant P, Sanchavanakit N, Supaphol P. Preparation and Characterization of Novel Bone Scaffolds Based on Electrospun Polycaprolactone, Macromolecular Bioscience, 6:70-7
Fibers Filled with Nanoparticles

[34] Phipps MC, Clem WC, Catledge SA, Xu Y. 2011, Mesenchymal Stem Cell Responses to bone-Mimetic Electrospun Matrices Composed of Polycaprolactone, Collagen I and Nanoparticulate Hydroxyapatite, *Plos one*, 6: 8 pages

[35] Rosmaninho R, Visser H, Melo L. 2004, Influence of the surface tension components of stainless steel on fouling caused by calcium phosphate, *Progr Colloid Polym Sci*, 123: 203-209

[35] Sabir MI, Xu X, Li Li. 2009, A review on biodegradable polymeric materials for bone tissue engineering applications, *J Mater Sci*, 44: 5713-5724

[37] Sill T. 2008, Electrospinning: Applications in drug delivery and tissue engineering. *Biomaterials*. 29(33): 1989-2006

[38] Starbova K, Krumov E, Karashanova D, Starbov N. 2009, Polyoxyethylene assisted electrospinning of nanofibers from calcium phosphate sol solution, *J Optoelectron Adv M*, 11: 1319-1322

[39] Sukigara S, Gandhi M, Ayutsede J, Micklus M, Ko F. 2003, Regeneration of Bombyx mori silk by electrospinning-part 1: processing parameters and geometric properties, *Polymer*, 44: 5721-5727

[40] Takeichi M. 1991, Cadherin cell adhesion receptors as a morphogenetic regulator, *Science*, 251: 1451-1455

[41] Teo WE. 2011, Technological advances in electrospinning of nanofibers, *Science and Technology of Advanced Materials*, 12:19

[42] Teo WE. 2011, A review on electrospinning design and nanofibre assemblie, *Nanotechnology*. 17: R89-R106

[43] Toure Y, Rouxhet PG, Dupont-Gillain CC, Sindie M. 2011, Influence of Soluble Polysaccharide on the Adherence of Particulate Soils, Heat Exchanger Cleaning Systems, 2011:219-226

[44] Vacanti, C. 2006, History of Tissue Engineering and A Glimpse Into Its Future. *Tissue Engineering*. 12.5: 1337-1142.

[45] Won Kim H, Hyoung Lee H, Knowles JC. 2006, Electrospinning biomedical nanocomposite fibers of hydroxyapatite/poly(lactic acid) for bone regeneration*, J Biomed Mater Res*,79: 643-649

[46] Wong S. 2010, An Investigation of Process Parameters to Optimize the Fiber Diameter of Electrospun Vascular Scaffolds through Experimental Design.

[47] Yamagata M, Saga S, Kato M, Bernfield M. 1993, Selective distributions of proteoglycans and their ligands in pericellular matrix of cultured fibroblasts, *J Cell Sci*, 106:55-65

[48] Yarin AL. 2005, Taylor cone and jetting from liquid droplets in electrospinning of nanofibers. *Journal of Applied Physics*. 90(9):4836-4846

[49] Yordem OS, Papila M, Menceloglu Y. 2008, Prediction of Electrospinning Parameters for Targeted nanofiber Diameter, Materials and Design, 29: 34-44

[50] Yordem OS, Papila M, Menceloglu YZ. 2008, Effects of electrospinning parameters on polyacrylonitrile nanofiber diameter: An investigation by response surface methodology, *Mater Design*, 29: 34-44

[51] Zhang H and Chen Z 2010, Fabrication and Characterization of Electrospun PLGA/MWNTs/Hydroxyapatite Biocomposite Scaffolds for Bone Tissue Engineering, *J Bioact Compat Polym*, 25: 241-259

[52] Ziabari M, Mottaghitalab V, Haghi AK. 2009, A new approach for optimization of electrospun nanofiber formation process, Korean Journal of Chemical Engineering, 27: 340-354

APPENDIX A

DATA COLLECTED JUNE 2011 - JULY 2013

Surface	Drops	Mean Contact Angle (Out of a set of 3)	Humidity (%)	Temp (Celsius)	Mean Surface Energy ϒ (mN/m) (Out of a set of 3)
PAA	8	27	13	19	96
PAA	12	41	13	19	88
PAA	16	37	13	19	75
Dex 70 KD	8	27	16	23	33
Dex 70 KD	12	23	18	28	112
Dex 70 KD	16	26	16	23	14
500 kD	8	38	13	19	43
500 kD	12	27	17	26	65
500 kD	16	25	18	28	76
70 KD / PAA	8	31	13	19	117
70 KD / PAA	12	30	15	21	48
70 KD / PAA	16	33	15	21	96
500 kD/PAA	8	30	13	19	54
500 kD/PAA	12	34	15	21	26
500 kD/PAA	16	32	15	21	35

Table 9: Surface tension calculated from the measured mean contact angle. Also shows the humidity and temperature measured during the time of measuring the mean contact angle. The drops show the number of drops of the specific solution dropped from the syringe needle unto the surface of a micro slide. The surface indicates the solution used to spin thin films.

	7%PAA	8.4%PAA	8.5%PAA
Distance (H) cm	**Calculated kV**	**Calculated kV**	**Calculated kV**
9	9.401499742	9.86037612	10.0819853
10	10.44611082	10.9559735	11.2022059
11	11.49072191	12.0515708	12.3224264
12	12.53533299	13.1471682	13.442647
13	13.57994407	14.2427655	14.5628676
14	14.62455515	15.3383628	15.6830882
15	15.66916624	16.4339602	16.8033088

Table 10: Shows the Voltage (kV) specifically calculated for 40wt% of 500kD Dextran and varying PAA v/v% Concentration. The kV was determined using the electrospinning equation using the calculated surface tension of the solution on a stainless steel surface and for a specific air-gap distance (H).

Surface	Drops	Ave C.A.	Humidity (%)	Temp (Celsius)	Surface Tension of water-Air interface for specific Temp	Surface Tension Between Liquid/Solid Interface for every individual droplet
Dex 70 KD	8	25.85	15	21	72.2577	17.70584389
Dex 70 KD	8	31.6	15	21	72.2577	1.123002669
70KD	8	23.45	18	28	71.1636	80.10977394
70KD	12	21.8	18	28	71.1636	142.0274738
70KD	12	22.95	18	28	71.1636	113.040678
70KD	12	23.45	18	28	71.1636	80.10977394
70KD	16	26	18	28	71.1636	26.12289211
Dex 70 KD	16	25.35	15	21	72.2577	1.600934063
Dex 70 KD	16	25.75	15	21	72.2577	13.23614727
500 kD	8	36.6	13	19	72.5703	39.32496467
500 kD	8	39	13	19	72.5703	52.94964241
500 kD	8	38.75	13	19	72.5703	36.24704275
500 KD	12	23.7	18	28	71.1636	62.50668036
500 KD	12	24.2	18	28	71.1636	29.91251784
500 KD	12	33.4	15	21	72.2577	101.3196109
500 KD	16	22.6	18	28	71.1636	130.6758895
500 KD	16	27.05	18	28	71.1636	96.46520766
500 KD	16	25.2	18	28	71.1636	1.297302224
PAA	8	39.6			72.5703	88.52220424
PAA	8	41.15	13	19	72.5703	134.126712
PAA	8	0				65
PAA	12	38.75	13	19	72.5703	28.94704275
PAA	12	41.9	13	19	72.5703	100.5221845
PAA	12	41.05	13	19	72.5703	135.9866369
PAA	16	43.3	13	19	72.5703	8.676286188
PAA	16	39.8	13	19	72.5703	101.6924559
PAA	16	29.1	13	19	72.5703	114.2075633
70kD/PAA	8	28.65	13	19	72.5703	139.6694965
70kD/PAA	8	29.75	13	19	72.5703	79.05321983
70kD/PAA	8	33.95	13	19	72.5703	131.7450545
70 KD / PAA	12	30.75	15	21	72.2577	15.34053913
70 KD / PAA	12	27.1	15	21	72.2577	100.0628606
70 KD / PAA	12	32.35	15	21	72.2577	29.19819733
70 KD / PAA	16	29.05	15	21	72.2577	123.7487305
70 KD / PAA	16	35.65	15	21	72.2577	105.4190916
70 KD / PAA	16	32.8	15	21	72.2577	58.74610052

Table 11: Shows the data taken for average contact angles of water on a surface made from various dex, paa, or dex-paa solutions. The drops indicate the number of drops used in making the thin film surface. The temperature and humidity indicate the parameters measured while measuring contact angles. The calculated surface tension of the water droplet and the thin film surface is also showed on the right of the table.